Science of the Total Environment 630 (2018) 1528–1543

Contents lists available at ScienceDirect

Science of the Total Environment

journal homepage: www.elsevier.com/locate/scitotenv

Implications of climate change on landslide hazard in Central Italy

Massimiliano Alvioli [a,*], Massimo Melillo [a], Fausto Guzzetti [a], Mauro Rossi [a], Elisa Palazzi [b], Jost von Hardenberg [b], Maria Teresa Brunetti [a], Silvia Peruccacci [a]

[a] Consiglio Nazionale delle Ricerche, Istituto di Ricerca per la Protezione Idrogeologica, via Madonna alta 126, I-06128 Perugia, Italy
[b] Consiglio Nazionale delle Ricerche, Istituto di Scienze dell'Atmosfera e del Clima, Corso Fiume 4, I-10133 Torino, Italy

HIGHLIGHTS

- We run a deterministic landslide model within rainfall events extracted from measured and downscaled precipitation data
- Downscaled precipitation data, obtained from WRF RPC4.5 model data, describes a historical period and afuture scenario
- We estimate landslide hazard modifications in terms of rainfall thresholds and size distributions.
- Rainfall thresholds are expected to change in Central Italy in the considered scenario
- Landslide size distributions, showing large statistical uncertainties, are not expected tochange

GRAPHICAL ABSTRACT

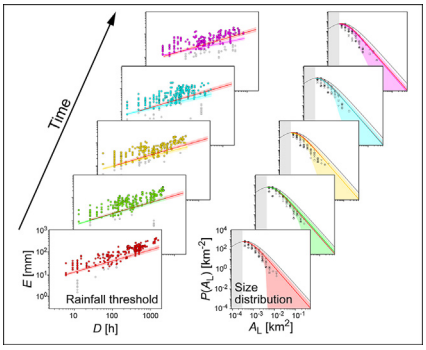

ARTICLE INFO

Article history:
Received 22 September 2017
Received in revised form 23 January 2018
Accepted 26 February 2018
Available online xxxx

Editor: R Ludwig

Keywords:
Landslide hazard
Climate change impact
Rainfall-induced landslides
Rainfall events
TRIGRS
RainFARM

ABSTRACT

The relation between climate change and its potential effects on the stability of slopes remains an open issue. For rainfall induced landslides, the point consists in determining the effects of the projected changes in the duration and amounts of rainfall that can initiate slope failures. We investigated the relationship between fine-scale climate projections obtained by downscaling and the expected modifications in landslide occurrence in Central Italy. We used rainfall measurements taken by 56 rain gauges in the 9-year period 2003–2011, and the RainFARM technique to generate downscaled synthetic rainfall fields from regional climate model projections for the 14-year calibration period 2002–2015, and for the 40-year projection period 2010–2049. Using a specific algorithm, we extracted a number of rainfall events, i.e. rainfall periods separated by dry periods of no or negligible amount of rain, from the measured and the synthetic rainfall series. Then, we used the selected rainfall events to forcethe Transient Rainfall Infiltration and Grid-Based Regional Slope-Stability Model TRIGRS v. 2.1. We analyzed the results in terms of variations (or lack of variations) in the rainfall thresholds for the possible initiation of landslides, in the probability distribution of landslide size (area), and in landslide hazard. Results showed that the downscaled rainfall fields obtained by RainFARM can be used to single out rainfall events, and to force the slope stability model. Results further showed that while the rainfall thresholds for landslide occurrence are expected to change in future scenarios, the probability distribution of landslide areas are not. We infer that landslide hazard in the study area is expected to change in response to the projected variations in the rainfall conditions. We expect our results to contribute to regional investigations of the expected impact of projected climate variations on slope stability conditions and on landslide hazards.

* Corresponding author at: CNR IRPI, via Madonna alta 126, I-06128 Perugia, Italy.
E-mail address: massimiliano.alvioli@irpi.cnr.it (M. Alvioli).

https://doi.org/10.1016/j.scitotenv.2018.02.315

1. Introduction

Establishing a relation between climate change and its potential climate effects on the occurrence – or lack of occurrence – of landslides in a given area remains an open issue (Gariano and Guzzetti, 2016). In fact, while climatic variables like temperature or precipitation can be simulated by numerical models and the corresponding level of confidence can be estimated (Giorgi and Lionello, 2008; Ciccarelli et al., 2008; Diffenbaugh and Field, 2013; IPCC, 2014; LoPresti et al., 2015; Turco et al., 2015), the way and the extent to which the projected climate changes may modify the response of single slopes or entire catchments, the frequency and extent of landslides, and the related variations in landslide hazard (Corominas, 2000; Coe and Godt, 2012; Hanson et al., 2012; Coe, 2016; Gariano and Guzzetti, 2016; Simonovic et al., 2016; Ciervo et al., 2017; Gariano et al., 2017b; Rianna et al., 2017), remain to be understood.

In this paper, we describe the results of an impact study aimed at establishing a cause-effect relationship between downscaled climate change projections and the expected modifications in landslide occurrence, and in the related landslide hazard, in an area of about 420 km^2 in Central Italy. For the study, we employed established techniques, procedures and models for (i) stochastic generation of synthetic downscaled rainfall fields from a regional climate model (Rebora et al., 2006a, 2006b; D'Onofrio et al., 2014), (ii) extraction of rainfall events from instrumental and synthetic rainfall series (Melillo et al., 2015, 2016), (iii) objective definition of rainfall thresholds from measurements of rainfall conditions that have resulted in landslides (Brunetti et al., 2010; Peruccacci et al., 2012), and (iv) spatially distributed, time-varying slope stability modelling forced by rainfall events (Baum et al., 2008; Alvioli et al., 2014; Alvioli and Baum, 2016).

The paper is organized as follows. First, we describe the study area, in the Upper Tiber River Basin (UTRB), Central Italy (Section 2). Next, we present the measured and the synthetic rainfall data series used in the study, the method used to single out rainfall events from the rainfall series, and the model used to ascertain the slope stability conditions, and their spatial and temporal variations (Section 3). This is followed by a description of the results of our modelling efforts (Section 4), and by a discussion of the results (Section 5). We conclude summarizing the main lessons learnt (Section 6). In an Appendix A, we give details on the procedures adopted to convert the pixel-based output of the models into landslide hazard metrics.

2. Study area

Our study area is included in the Upper Tiber River Basin (UTRB) that extends for about 4100 km^2 in Central Italy (Fig. 1). In the catchment, elevation ranges from 163 m to 1571 m at M. Pennino, along the divide between the Adriatic Sea and the Tyrrhenian Sea, and terrain gradient computed from a 10 m × 10 m Digital Elevation Model (DEM) ranges from almost zero along the plain of the Tiber River and its major tributaries, to >60° in the mountains and the steepest hills. Four lithological complexes, or groups of rock units (Cardinali et al., 2001), crop out in the area, each comprising different sedimentary rock types varying in strength from hard to weak and soft rocks (Guzzetti et al., 1996, 2008a). Soils reflect the lithological types, and range in thickness from <20 cm to >1.5 m. Climate is of Mediterranean type, with cold winters and hot summers. Rainfall occurs mainly from October to December and from February to April. Snow falls every year in the mountains and about every five years in the lowlands (Guzzetti et al., 2008a). Due to the lithological and morphological settings, and to the meteorological and climatic conditions, landslides are abundant in the UTRB, and are particularly numerous in the continental, post-orogenic sediments, which extend for 422 km^2, consisting primarily of clay and silt, and subordinately of sand and gravel, deposited in a continental, lake environment (Cardinali et al., 2001; Guzzetti et al., 2008a).

3. Data and models

3.1. Measured rainfall series

We used rainfall measurements taken by a network of 56 rain gauges (yellow dots in Fig. 1) in the UTRB in the 9-year period from 1 January 2003 to 31 December 2011. The network is part of a larger national network operated by the Italian regional governments and the Italian national Department for Civil Protection. In the area, the temporal sampling of the rainfall data varied from 1 to 60 min, with the majority of the measurements taken every 30 min, and the measurement accuracy was in the range between 0.2 mm and 1.0 mm. A specific procedure was used to evaluate and rank the reliability of the rain gauge sensors, allowing to identify missing data, errors and periods of proper functioning in each rain gauge data series. In the 9-year period 2003–2011, the mean annual precipitation (MAP) measured at the 56 rain gauges was 860 mm (blue histogram in Fig. 2), with a minimum value of 583 mm in 2003, and a maximum value of 1463 mm in 2010. Rainfall measurements at rain gauge locations were interpolated to produce grids suitable for use in TRIGRS at 1 km spatial resolution, using an inverse distance criterion.

3.2. Synthetic rainfall series

Various techniques exist to downscale large-scale rainfall fields such as those produced by Global and Regional Climate Models (GCMs and RCMs) to the high temporal and spatial resolutions required by local impact studies. Amongst them, statistical and stochastic downscaling techniques proved particularly effective (Bordoy and Burlando, 2014). For our study, we used synthetic rainfall data obtained by the Rainfall Downscaling by a Filtered AutoRegressive Model (RainFARM) technique (Rebora et al., 2006a, 2006b), a stochastic procedure belonging to the family of "metagaussian models", based on nonlinear filtering of the output of a linear autoregressive process, whose properties are derived from the information available at the large scales. The RainFARM technique was originally developed for the spatial and temporal downscaling of individual precipitation events on the time scales typical of meteorological events (Rebora et al., 2006a, 2006b), and was next updated to cope with longer climatic timescales, which required the application of a purely spatial downscaling (D'Onofrio et al., 2014).

The RainFARM technique has been used for different kinds of studies, including (i) the analysis of the sensitivity of a distributed hydrological model to the variability of the spatio-temporal rainfall distribution (Gabellani et al., 2007), (ii) the estimation of the uncertainty in flood predictions (Rebora et al., 2006a), (iii) the assessment of the main uncertainty sources in ensemble precipitation forecasts (von Hardenberg et al., 2007), and (iv) the quantification of sampling errors for the verification of meteorological forecasts against rain gauge observations (Brussolo et al., 2008). In this work RainFARM is used for the first time for the study of the impact of precipitation changes on landslide occurrence.

We applied RainFARM to the output of a set of simulations preformed with the state-of-the-art non-hydrostatic Weather Research and Forecasting (WRF) RCM run over the entire European domain at 0.11° spatial resolution (~12 km) and 3-h temporal resolution for a historical period (1979–2005) and a scenario period (2006–2049) using RCP4.5 radiative forcing (Thomson et al., 2011). The simulation used the WSM6 (Hong and Lim, 2006) microphysics parameterization and the convective scheme of Kain and Fritsch (1990), and is described in more detail in Pieri et al. (2015) and in von Hardenberg et al. (2015).

Application of RainFARM to WRF allowed us to produce gridded precipitation datasets covering the UTRB at 1 km × 1 km spatial resolution and at the same temporal resolution as the original data. We then sampled the grids corresponding to the location of each rain gauge (Fig. 1), producing 56 synthetic rainfall series (one series for each rain gauge) for the 9-year (past) calibration period 2002–2015, and the 40-year projection period 2010–2049.

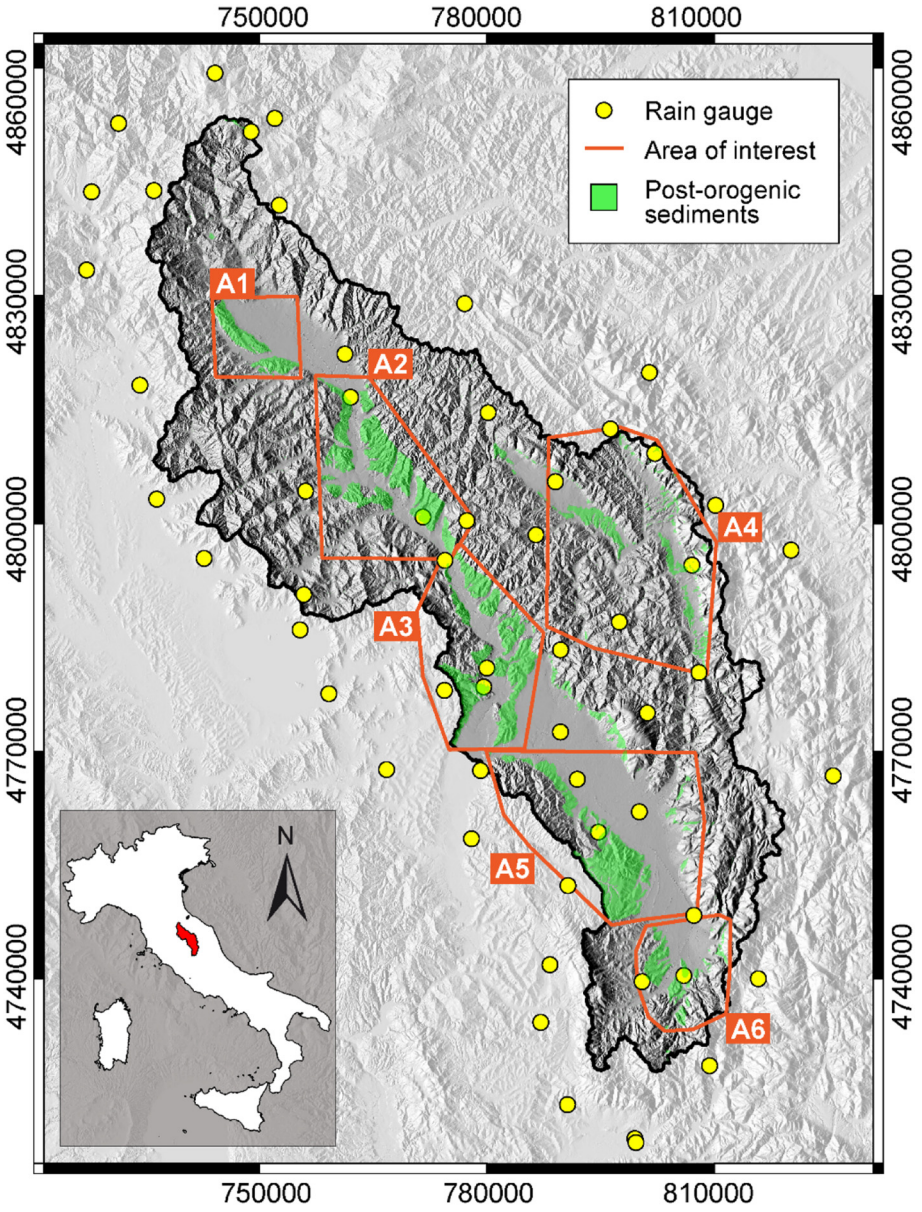

Fig. 1. The Upper Tiber River basin (UTRB), Central Italy. Background is a shaded relief map calculated using TINITALY, the 10 m × 10 m DEM used in this work (Tarquini et al., 2012). Yellow dots show locations of 56 rain gauges used in the study. Green areas show the continental, post-orogenic sediments were the TRIGRS simulations were performed. Orange lines encompass the six sub-areas referred to in the paper. (For interpretation of the references to colour in this figure legend, the reader is referred to the web version of this article.) (For interpretation of the references to colour in this figure legend, the reader is referred to the web version of this article.)

The stochastic downscaling method employed in this work implicitly takes into account orographic effects at the scale of the original field (about 12 km in our case), since it preserves the average precipitation volumes at that scale. The issue of orographic effects, investigated recently by different authors (e.g., Harris et al., 1996; Badas et al., 2005), is particularly important when downscaling is performed starting from global climate models at coarse resolutions (D'Onofrio et al., 2014). When starting from 30 km scales or larger, most of the orographic effects may be already captured by the dynamical downscaling procedure. The RainFARM procedure provides a good representation of sub-grid precipitation extremes (D'Onofrio et al., 2014).

3.3. Extraction of rainfall events

In general, rainfall time series consist of rainfall measurements (M) or rainfall synthetic data (S_P for the past, and S_F for the future) cumulated over continuous, fixed time intervals (e.g., minutes, hours, days). However, landslides are known to be triggered by rainfall events R_E (Aleotti, 2004; Guzzetti et al., 2007; Brunetti et al., 2010; Berti et al., 2012) i.e., rainfall periods of different duration and cumulated precipitation separated by dry periods with no rain, or with a negligible amount of rain (Guo, 2002; Guzzetti et al., 2007; Brunetti et al., 2010; Saito et al., 2010; Shamsudin et al., 2010; Melillo et al., 2015).

Identification of R_E from rainfall series is not trivial. To single out R_E in our measured and synthetic rainfall series, we adopted the algorithm proposed by Melillo et al. (2015, 2016), which was devised specifically for the detection and characterization of rainfall events that have triggered known landslides from measured hourly rainfall series. The algorithm depends on a number of parameters, the most important of which being the duration (in hours) of the dry period that separates two consecutive R_E. The length of the dry period depends on seasonal conditions. In the Mediterranean region, the dry period is typically shorter in the "warm" and dry spring-summer period from May to September, and is longer in the "cold" and wet autumn-winter period from October

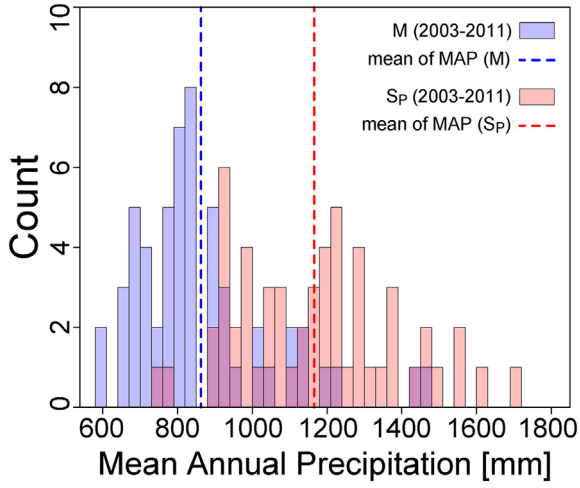

Fig. 2. Distribution of the mean annual precipitation (MAP) at the 56 rain gauges used in the study, for the measured, M (blue), and the synthetic, S_P (red), rainfall data. See Fig. 1 for the location of the rain gauges for the 9-year overlapping period of the two data sets, between 2003 and 2011. Vertical dashed lines show mean MAP values for the different periods. (For interpretation of the references to colour in this figure legend, the reader is referred to the web version of this article.) (For interpretation of the references to colour in this figure legend, the reader is referred to the web version of this article.)

to April (Brunetti et al., 2010; Melillo et al., 2015, 2016; Peruccacci et al., 2017). Following Melillo et al. (2015), we distinguished a minimum dry period for the "warm" (May–September) period C_W, and a minimum dry period for the "cold" (October–April) period, C_C. To investigate the sensitivity of the results to the model parameters, we repeated the selection of measured and synthetic R_E nine times, corresponding to nine different combinations of C_C and C_W. We considered (C_C-15%, C_C, C_C + 15%) combined with (C_W-15%, C_W, C_W + 15%), were C_C = 48 h and C_W = 96 h are the values used by Melillo et al. (2015) in Sicily, Southern Italy. Using different values for the input parameters also helps investigating possible dependence of their numerical values on the specific study area.

3.4. Modelling of slope stability

To determine the stability conditions of the slopes in our study area, forced by time-varying rainfall inputs, we used TRIGRS v. 2.1 (Alvioli and Baum, 2016), an updated, parallel implementation of the Transient Rainfall Infiltration and Grid-Based Regional Slope-Stability Model v. 2.0 (TRIGRS) for the timing and distribution of rainfall-induced shallow landslides (Baum et al., 2008).

TRIGRS performs spatially-distributed, time-varying slope stability simulations using information on (i) the geometrical and the mechanical properties of the slopes, and (ii) the rainfall history that may cause a slope to fail. To represent topography in the UTRB, we used TINITALY (Tarquini et al., 2012) – a 10 m × 10 m DEM produced for the whole of Italy from heterogeneous vector elevation data, consisting mostly in contour lines and elevation points obtained from several sources – which we considered adequate for our regional slope stability modelling (Alvioli et al., 2014; Raia et al., 2014). Following Alvioli et al. (2014), we limited the slope stability simulations to the continental, post-orogenic sediment complex (green areas in Fig. 1), where landslides are more abundant and frequent (Cardinali et al., 2001; Guzzetti et al., 2008a). The values used to represent the geo-mechanical properties of the sediments in the post-orogenic complex were the same used by Alvioli et al. (2014) i.e., cohesion, c = 3.0 kPa; internal friction angle, $\varphi = 15°$; wet soil unit weight, γ_S = 15,000 Nm^{-3}; diffusivity, $D_0 = 4.7 \cdot 10^{-3}$ m^2 s^{-1}; and saturated hydraulic conductivity, $K_S = 10^{-4}$ ms^{-1}. The soil setting of the green areas in Fig. 1 is a rather heterogeneous one. In TRIGRS simulations we set numerical values of the geotechnical properties correspond to a worst case scenario, in which the three most important parameters (cohesion, friction angle and hydraulic conductivity) favour landslides. This is also justified by our final aim, that is, to provide relative results. Possible biases introduced by peculiar choices, for example the particular values of the geotechnical parameters, cancel out in the comparison of simulations corresponding to the future and past periods. To limit the model complexity, and to reduce the computer processing effort, we used the simplifying assumption of a fully saturated, infinite soil depth slope (Baum et al., 2008; Alvioli and Baum, 2016). We maintain that the simplifications are reasonable for the aim of this work.

We performed the simulations using information on R_E singled out from the measured (M) and the synthetic (S_P and S_F) rainfall series using the algorithm proposed by Melillo et al. (2015, 2016). TRIGRS requires spatially distributed rainfall information in the form of grids, e.g. one grid for each 3-hour processing step in our case, (Baum et al., 2008; Alvioli and Baum, 2016). Thus, we transformed the synthetic rainfall data provided downscaled by RainFARM at 1 km × 1 km resolution to the 10 m × 10 m resolution of the DEM used for slope stability modelling. For the rainfall measurements obtained at the 56 station locations (Fig. 1), the rainfall information was also interpolated to the 10 m × 10 m DEM resolution, using an inverse distance algorithm. For convenience, we set to 3 h the time step for the slope stability simulations. This corresponds to the temporal resolution of the downscaled rainfall data. In this 3-hour period, rainfall rate was considered to be constant, a reasonable assumption for the aim of this work (Alvioli et al., 2014; Raia et al., 2014).

Since the simulation of a single rainfall grid with at 10 m × 10 m resolution covering the entire UTRB required about 700 MB of disk storage, and many grids (one every 3 h) were necessary to process even relatively short R_E lasting from a few hours to a few days, a complete simulation covering the entire UTRB for the whole examined period (about 50 years) was prohibitive, and two approximations were applied. First, we split the study area into six sub-areas (orange polygons in Fig. 1), and we performed separate model runs for each of them. Second, we selected subsets of all rainfall events singled out by the event selection procedure, and specifically: (i) 50 R_E singled out from the measured rainfall series from 2003 to 2011, (ii) 50 R_E from the synthetic rainfall series in the 14-year calibration period 2002–2015, and (iii) 50 R_E from the synthetic rainfall series for each decade (10-year period) from 2010 to 2049. This procedure gave rise to a total of 300 R_E. The first simplification reduced considerably the amount of computer memory, storage and I/O operations required to perform the numerical simulations, and the second simplification reduced the number of model runs, keeping them representative of the ensemble of the rainfall events in each of the considered modelling periods.

We analyzed the TRIGRS model outputs in terms of the spatial distribution of the "factor of safety" FS, an index expressing the ratio between the local resisting (R) and driving (T) forces, FS = R/T. Values of FS smaller than unity correspond to $R < T$, and denote instability of the grid cell (Baum et al., 2008; Alvioli et al., 2014; Raia et al., 2014; Alvioli and Baum, 2016; Viet et al., 2018). The values of the FS were computed and stored at each 3-hour time step. Due to storage limitations, all the grids were discarded after the analysis of each single event was completed. Adopting the same criteria proposed by Alvioli et al. (2014), we examined the spatial and the temporal trends of the FS tracking the number of the unstable cells with FS < 1.0, and the number of "landslides" i.e., of clusters of contiguous cells with FS < 1.0. Different approaches exist for a sound definition of modelled landslides areas starting from the two-dimensional FS grid (Bellugi et al., 2015) or using a three-dimensional FS definition (Reid et al., 2015; Viet et al., 2018); however, these are beyond the scope of this work.

4. Results

We present the results of our modelling effort in three complementary steps. First, we compare the rainfall events singled out from the

Table 1
Rainfall events (R_E), for six periods, extracted from the measured (M) and the synthetic (S_P and S_F) rainfall series using the algorithm proposed by Melillo et al. (2015, 2016). In each period, #R_E is the number of rainfall events, R_E the number of rainfall events per year, $R_{E\text{-}G}$ the number of R_E per year and per rain gauge, E_{min} (E_{max}) the minimum (maximum) cumulated event rainfall (in mm) and D_{min} (D_{max}) the minimum (maximum) rainfall duration (in hours).

ID	Period	#R_E	R_E	$R_{E\text{-}G}$	E_{min}	E_{max}	D_{min}	D_{max}
M	2003–2011	12,179	1353	24	1	654	3	1362
S_P	2002–2015	23,641	1689	30	1	670	3	1941
S_{F1}	2010–2019	21,182	2118	38	1	597	3	1047
S_{F2}	2020–2029	21,157	2116	38	1	355	3	918
S_{F3}	2030–2039	19,942	1994	36	1	379	3	1221
S_{F4}	2040–2049	19,797	1980	34	1	506	3	1344

measured and the synthetic rainfall series. Second, we calculate synthetic (modelled) rainfall thresholds for the rainfall conditions that have resulted in slope instability, and we compare them with an existing empirical threshold for possible landslide occurrence in the same geographical area. Third, we examine the statistics of landslide area A_L, known to represent a fingerprint of the population of landslides (Guzzetti et al., 2002).

4.1. Comparison of observed and synthetic rainfall events

Fig. 2 shows the frequency distribution of the MAP at the 56 rain gauges locations used in this study for the measured rainfall series M and for the synthetic rainfall series S_P, in the 9-year period 2003–2011 for which both rainfall series are available. Inspection of Fig. 2 reveals that the synthetic series S_P exhibits larger MAP values. Regional climate models over the Mediterranean region often exhibit a "wet bias" over orographic reliefs as shown by Kotlarski et al. (2014) for the recent Coordinated Regional Climate Downscaling Experiment (CORDEX) simulations. The WRF simulations downscaled in this work show a similar behavior as well, and present an overestimate of precipitation over the European and the Alpine regions (Pieri et al., 2015). By construction the RainFARM downscaling procedure maintains the same average precipitation as its large-scale driver, so it does not correct the "wet bias", but it may contribute to extend the range of high precipitation values found at high resolution (D'Onofrio et al., 2014). Due to the limited duration of our observations (9 years) and to the difficulties and uncertainties inherent in any bias correction method (Ehret et al., 2012), we preferred not to apply a bias correction to the WRF data and we took this into consideration in the evaluation and discussion of results. We further stress that performing TRIGRS simulations within individual rainfall events, lasting from a few hours to a few weeks, strongly reduces the discrepancy found on the one-year scale shown in Fig. 2.

For the sets of R_E extracted from the measured rainfall in the 9-year period 2003–2011 (M), and the synthetic rainfall series in the 48-year period 2002–2049 (S_{F1}-S_{F4}), using the algorithm proposed by Melillo et al. (2015, 2016), we calculated the rainfall duration D (in hours) and the cumulated event rainfall E (in mm); two parameters known to control the initiation of landslides (Guzzetti et al., 2007, 2008b; Brunetti et al., 2010; Peruccacci et al., 2012, 2017). Table 1 summarizes statistics for the R_E, for the different periods. We note that the synthetic data for the four 2010–2049 decades contain about 20% more events than the events identified using the measured rainfall data in the period 2003–2011, and the synthetic rainfall data in the period 2002–2015.

We determined the empirical cumulative density function (ECDF) for the rainfall duration D, and for the cumulated event rainfall E. Results are portrayed in Fig. 3, showing that the synthetic data (red shaded areas) have a slightly larger variability than the measured data (blue shaded areas), for both the rainfall duration D and the cumulated event rainfall E, while central values are very similar. The variability is slightly larger for the rainfall duration D, than for the cumulated event rainfall E. Therefore, from now on, we adopted R_E obtained with the central values $C_W = 48$ h and $C_C = 96$ h, taken from Melillo et al. (2015). For the synthetic rainfall data, we also computed the ECDFs for the four successive decades in the period 2010–2049 (Fig. 4). Inspection of the decadal ECDFs does not reveal significant differences in the statistics of the rainfall duration D, or the cumulated event rainfall E.

To perform slope stability simulations, we devised a procedure to select a small subset of representative R_E from the entire set of events. For each of the six considered periods (Table 1), we selected randomly 50 R_E, and we repeated the selection 5000 times, to obtain 5000 sets each with 50 R_E. We then calculated the average ECDF curve, and selected the single ECDF that was closest to the calculated average curve. Results are summarized in Fig. 5, where the random ensemble is represented by grey curves, the calculated average by the black dotted curves, and the selected ECDFs by colored curves. The corresponding six sets of 50 R_E, one set for each period, where then used to force the spatially distributed, time-varying slope stability modelling performed by TRIGRS.

4.2. Slope stability modelling with TRIGRS

We performed a total of 1800 spatially distributed, time-varying slope stability simulations, including: (i) 300 simulations (50 $R_E \times 6$ sub-areas) using the measured rainfall data (M), (ii) 300 simulations (50 $R_E \times 6$ sub-areas) using the downscaled synthetic rainfall data in the 14-year calibration period 2002–2015 (S_P), and (iii) 1200

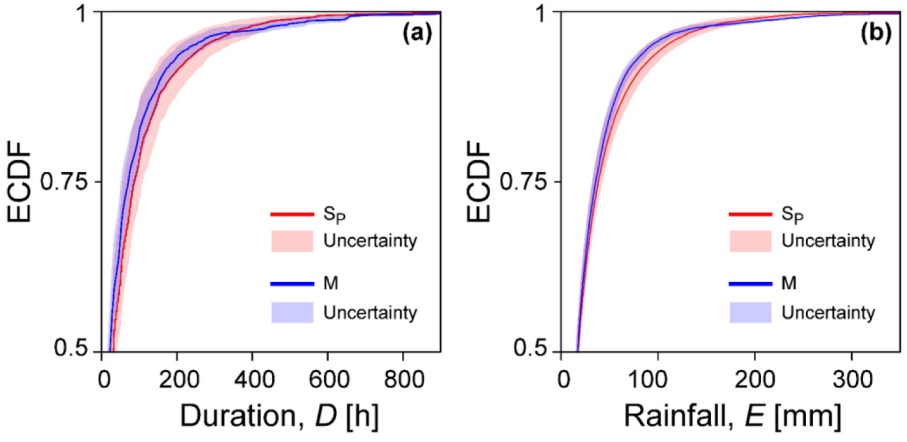

Fig. 3. Comparison of empirical cumulative density function (ECDF) for (a) the rainfall event duration D (in hours) and (b) the cumulated event rainfall E (in mm), calculated for the measured (M, blue) and the synthetic past (S_P, red) rainfall events. Bands in colour show the uncertainty associated with the algorithm parameters of Melillo et al. (2015, 2016). Solid curves were obtained using $C_W = 48$ and $C_C = 96$. (For interpretation of the references to colour in this figure legend, the reader is referred to the web version of this article.) (For interpretation of the references to colour in this figure legend, the reader is referred to the web version of this article.)

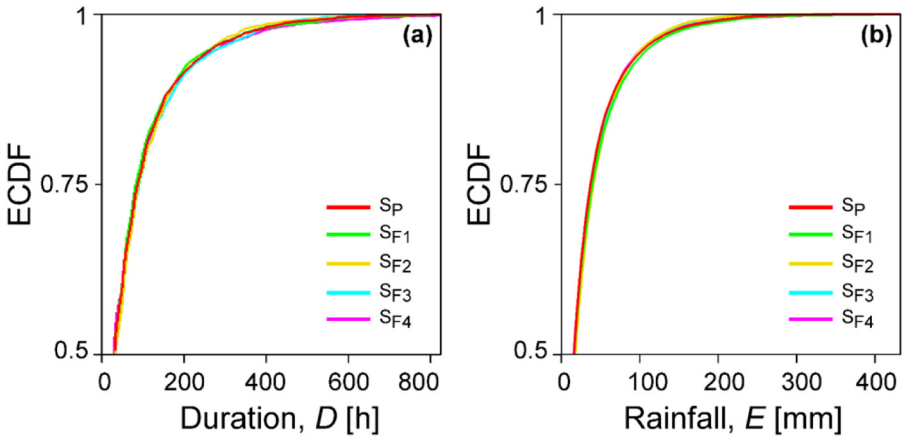

Fig. 4. Comparison of empirical cumulative density function (ECDF) for (a) the rainfall event duration D (in hours) and (b) the cumulated event rainfall E (in mm), calculated for synthetic past (S_P, red) rainfall events (2002–2015) with synthetic future (projected) rainfall events (S_{F1}, green (2010–2019); S_{F2}, yellow (2020–2029); S_{F3}, cyan (2030–2039); S_{F4}, magenta (2040–2049)). All curves were obtained using $C_W = 48$ and $C_C = 96$. (For interpretation of the references to colour in this figure legend, the reader is referred to the web version of this article.) (For interpretation of the references to colour in this figure legend, the reader is referred to the web version of this article.)

simulations (50 R_E × 6 sub-areas × 4 decades) using the downscaled synthetic rainfall data for the four decades in 40-year period 2010–2049 (S_{F1}- S_{F4}). Each model run (one simulation) required between 1 and 10 h of computer time, and used between 10 and 30 processors per parallel run, between a few and about 100 GB of RAM, and between 1 and about 200 GB of storage space, depending on the length of the considered R_E. After each run, we analyzed the output maps and calculated relevant summary quantities, i.e. the number of unstable cells and the number of landslides (neighboring clusters of failing cells), at each time step and for each of the six sub-areas. The maps were deleted after the analysis, and the only summary quantities were stored for each simulated event, along with the corresponding duration and cumulative rainfall at each time step.

For illustrative purposes, Fig. 6 shows the result of a single simulation taken from the S_P ensemble, and specifically the simulation of the longest R_E in the S_P series. The synthetic event lasted 1443 h (60 days), corresponding to 481 time modelling steps in TRIGRS. Fig. 6a shows the temporal evolution of the total number of unstable cells (i.e., grid cells with FS < 1.0) in the six considered sub-areas, and Fig. 6b shows the temporal variation of the slope stability conditions in response to the time-varying rainfall, for one of the study areas (i.e., A1 in Fig. 1). Inspection of Fig. 6b reveals that shortly after a rainfall peak, shown by a rapid increase in the rainfall intensity, the number of the unstable cells increases rapidly. Then, gradually, the number of the unstable cells decreases to return to a condition of general stability in the study area, characterized by a large number of grid cells with FS ≥ 1.0. Fig. 6c further compares the temporal evolution of the number of modelled "landslides", defined as clusters of adjacent cells with FS < 1.0 (violet line) (Alvioli et al., 2014), to the total number of unstable cells (red line), during the rainfall event. We observe that the number of landslides changes as a function of time in larger discrete steps than the number of the individual cells. This is consistent with our definition of a landslide as cluster of neighboring unstable cells. In the simulation, the maximum number of unstable cells occurred almost at the end of the rainfall event, and corresponds to the red dot with $E = 425$ mm and $D = 1428$ h (two months) in Fig. 7b.

4.2.1. Rainfall thresholds

We used the rainfall duration D (in hours) and the event cumulated rainfall E (in mm) computed for the rainfall events extracted from the different rainfall series, to reconstruct rainfall thresholds that represent the minimum (D, E) rainfall conditions above which landslides are expected to occur in the UTRB, with a given probability (Guzzetti et al., 2007, 2008a; Brunetti et al., 2010; Peruccacci et al., 2012). To select the R_E, we adopted the algorithm proposed by Melillo et al. (2015, 2016) that requires information on the "time of occurrence" of the landslide. For this work, we set the "time of occurrence" of the landslide to coincide with the time in any given simulation when the maximum number of cells were predicted to fail (FS < 1.0). As a consequence, the corresponding rainfall duration and the event cumulated rainfall represent the (D, E) rainfall conditions that have caused the modelled landslide. In this way, we obtained 50 (D, E) pairs for each considered period, and for each of the six sub-areas, corresponding to a total of (i) 300 (D, E) pairs for each of the "past" periods (M, 2003–2011; S_P, 2002–2015) and of (ii) 1200 (D, E) pairs for the "future" period (S_{F1}-S_{F4}, 2010–2049). We note that the number of (D, E) pairs used in Fig. 7 exceeds the number considered adequate to construct objective thresholds with an acceptable level of uncertainty (Peruccacci et al., 2012, 2017).

To obtain rainfall thresholds, we used the procedure proposed by Brunetti et al. (2010) and modified by Peruccacci et al. (2012), which was designed to determine objective and reproducible thresholds from a distribution of (D, E) pairs in a Cartesian DE plane. The procedure assumes that the threshold curve takes the form of a power-law, $E = \alpha D^{\gamma}$ with the parameters α and γ representing a constant factor and the scaling exponent of the threshold curve, respectively. Following Brunetti et al. (2010) and Peruccacci et al. (2012), we defined 5% exceedance probability thresholds (T_5) i.e., threshold curves that leave 5% of the (D, E) pairs below the threshold line.

We used the results obtained from the observed data set (M) to calibrate the procedure for the calculation of threshold curves for the synthetic data sets (S_P and S_F). Some of the (D, E) rainfall conditions resulting from the TRIGRS simulations lie well below the empirical threshold curve defined by Peruccacci et al. (2012) in central Italy ($T_{5,AMU}$, the 5% threshold valid for Abruzzo, Marche and Umbria regions). We considered these conditions not representative of overt slope instability conditions, and we discarded them (see Appendix A). We used the remaining valid points to calculate the 5% threshold for the observed data set ($T_{5,M}$ in Fig. 7a). We used the same criterion to discard a few rainfall conditions in the synthetic data sets (e.g., the S_P data set in Fig. 7b and the S_F data sets in Fig. 8). We consider this a calibration procedure to calculate the corresponding 5% thresholds, $T_{5,S}$ curves. Fig. 7a shows that the $T_{5,M}$ is defined in the range $3 \le D \le 939$ h and $7 \le E \le 276$ mm. Fig. 7b shows that the $T_{5,SP}$ is defined in the range $6 \le D \le 1614$ h and $9 \le E \le 425$ mm. The $T_{5,M}$ and $T_{5,SP}$ curves are very similar and can be considered equivalent.

We defined thresholds for the synthetic S_{F1}, S_{F2}, S_{F3}, and S_{F4} data sets ($T_{5,SF1}$, $T_{5,SF2}$, $T_{5,SF3}$ and $T_{5,SF4}$ in Fig. 8), in order to investigate threshold variations in the future. For consistency, we compared these thresholds to $T_{5,SP}$, and not to $T_{5,M}$, though $T_{5,M}$ and $T_{5,SP}$ are equivalent. We observe

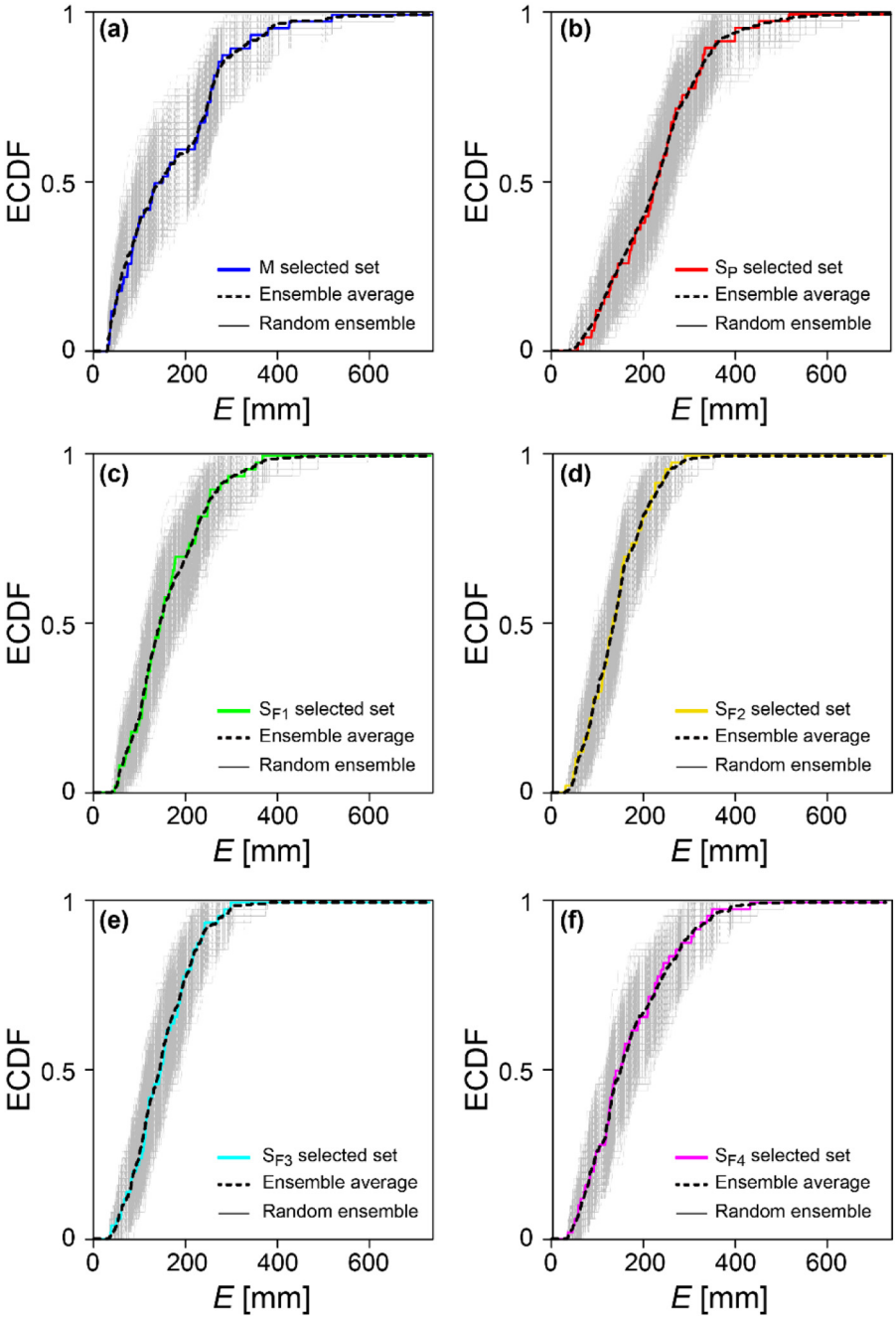

Fig. 5. Representative subsets of rainfall events for the six different data sets listed in Table 1. Grey curves show an ensemble of 5000 sets of 50 events, each selected randomly from the corresponding total number of events extracted from each data set. Black dotted curves show the average ECDF for the corresponding ensemble. Colored curves are the selected sets (each containing 50 events) closest to the ensemble average, with respect to their root mean square deviation.

that $T_{5,SP}$ and $T_{5,SF1}$ curves coincide, even if they are defined in different ranges. This is consistent with the fact that the two periods overlap between 2010 and 2015. Results from the future decades indicate that the slope of the synthetic thresholds progressively decreases from 0.5 to 0.35, and the intercept increases slightly from $\log_{10}(3.8)$ to $\log_{10}(6.0)$. This highlights a sizable effect of the projected climate change on the rainfall thresholds that can initiate landslides in our study area.

4.2.2. Landslide area distributions

The probability of landslide area $P(A_L)$ is known to obey a typical distribution, with the probability that increases with landslide area up to a maximum value (the so called "rollover"), and then decreases rapidly following a power law (Guzzetti et al., 2002; Malamud et al., 2004). This typical distribution is well approximated by functions (Hovius et al., 1997; Malamud et al., 2004) whose parameters depend on the mechanical properties of the soils and rocks where the landslides occur (Katz and Aharonov, 2006; Stark and Guzzetti, 2009; Klar et al., 2011). It remains uncertain if $P(A_L)$ will change in response to climate changes (Gariano and Guzzetti, 2016). To help answer this question, we calculated the area of the landslides identified by the numerical slope-stability simulations, and we determined the probability density function of these landslide areas.

For the purpose, the individual "landslides" were first singled out from the FS maps produced by TRIGRS. This was obtained clustering

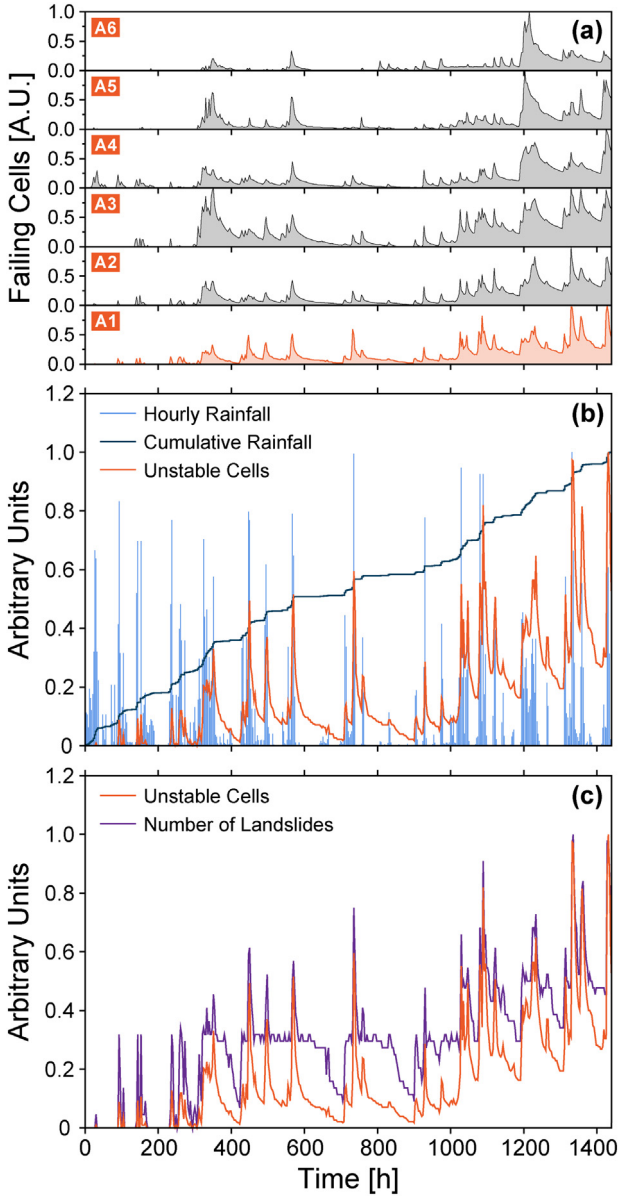

Fig. 6. A sample, very long simulated event from the S_P ensemble. All curves are scaled to their maximum value, in the considered time interval, to compare their time dependence, with 3-h time steps. (a) plots show number of failing cells predicted by TRIGRS, for the six sub-areas referred to in the paper. The maximum number of unstable cells in the areas labelled from1 to 6 occurs after 1428 h, 1329 h, 1329 h, 1425 h, 1203 h and 1215 h, respectively. Panels (b) and (c) show, for the sub-area A1: panel (b), the rainfall intensity averaged over the area at each time step, the cumulative of the rainfall intensity, and the number of failing cells; panel (c), the number of landslides (i.e., clusters of adjacent failing cells) compared to the number of failing cells. In this event, the maximum number of failing cells (i.e., the synthetic landslide) occurs almost at the end of the event, that corresponds to the point $(D,E) = (1428\ \text{h}, 425\ \text{mm})$.

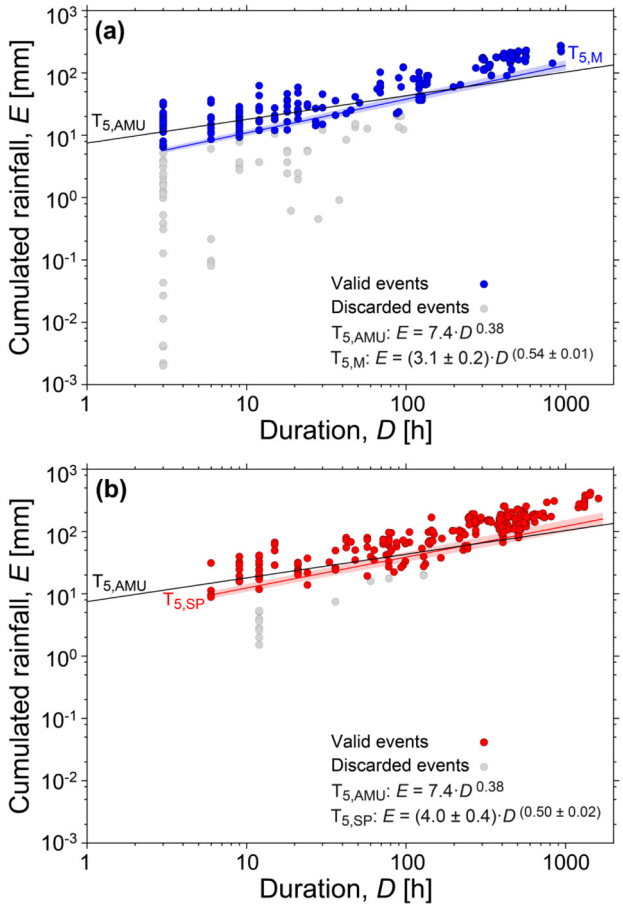

Fig. 7. Cumulated event rainfall E (mm) vs. rainfall duration D (h) conditions that have generated the largest number of unstable cells in the simulated events for the M (blue dots in Fig. 7a) and the S_P (red dots Fig. 7b) data sets. Grey dots show rainfall conditions unlikely responsible for the observed failures. Colored curves are the corresponding 5% thresholds $T_{5,M}$ (Fig. 7a) and $T_{5,SP}$ (Fig. 7b). Shaded areas show uncertainty associated to the new thresholds. $T_{5,AMU}$ is the threshold defined by Peruccacci et al. (2012) valid for the same geographical area. Data shown in log–log coordinates. (For interpretation of the references to colour in this figure legend, the reader is referred to the web version of this article.) (For interpretation of the references to colour in this figure legend, the reader is referred to the web version of this article.)

adjacent cells having FS < 1 (Alvioli et al., 2014). Next, the area of each landslide was obtained summing the area of all the adjacent 10 m × 10 m grid cells forming the landslide. In this way, we identified an average of 1277 landslides per event in the simulations performed using the measured data set, and about 600–800 landslides per event for each of the simulations performed using the synthetic sets, highlighting a sharp difference between the two. In Table 2 we report complete statistics of the slope stability simulations performed by TRIGRS. Lastly, for each of the six data sets (M, S_P, S_{F1}, S_{F2}, S_{F3}, S_{F4}) we fitted the empirical distributions of landslide areas with the inverse Gamma function proposed by Malamud et al. (2004) to describe the probability density function of landslide areas, $P(A_L)$. Results are summarized in Fig. 9, for the different considered periods.

Visual inspection of Fig. 9 reveals that the probability density of the area of the landslides singled out from the TRIGRS simulations, for the different periods, follows well the expected power law decaying behavior, for $A_L > 300\ \text{m}^2$. However, the empirical distributions fail to reproduce the "rollover" typical of empirical landslide data sets obtained from accurate landslide event inventory maps (Malamud et al., 2004). The result is not new (Alvioli et al., 2014; Hergarten, 2012), but the reasons for the result are not fully known. In our case, they may depend on the inherent one-dimensional formulation of the slope-stability model adopted in TRIGRS that does not provide an accurate way of clustering adjacent unstable pixels into a single landslide. For this reason, we discarded simulation results for $A_L < 300\ \text{m}^2$ (shaded area in Fig. 9), following the procedure that we consider a calibration step described in the Appendix A.

Further inspection of Fig. 9 reveals that the probability densities of landslide areas obtained forcing the TRIGRS model with synthetic R_E (Fig. 9b-f), for $A_L > 300\ \text{m}^2$, are nearly identical to the probability density of the modelled landslide areas obtained using the measured R_E (M, Fig. 9a). We conclude that in the considered period, and in our study area, we do not expect the probability density of landslide area to

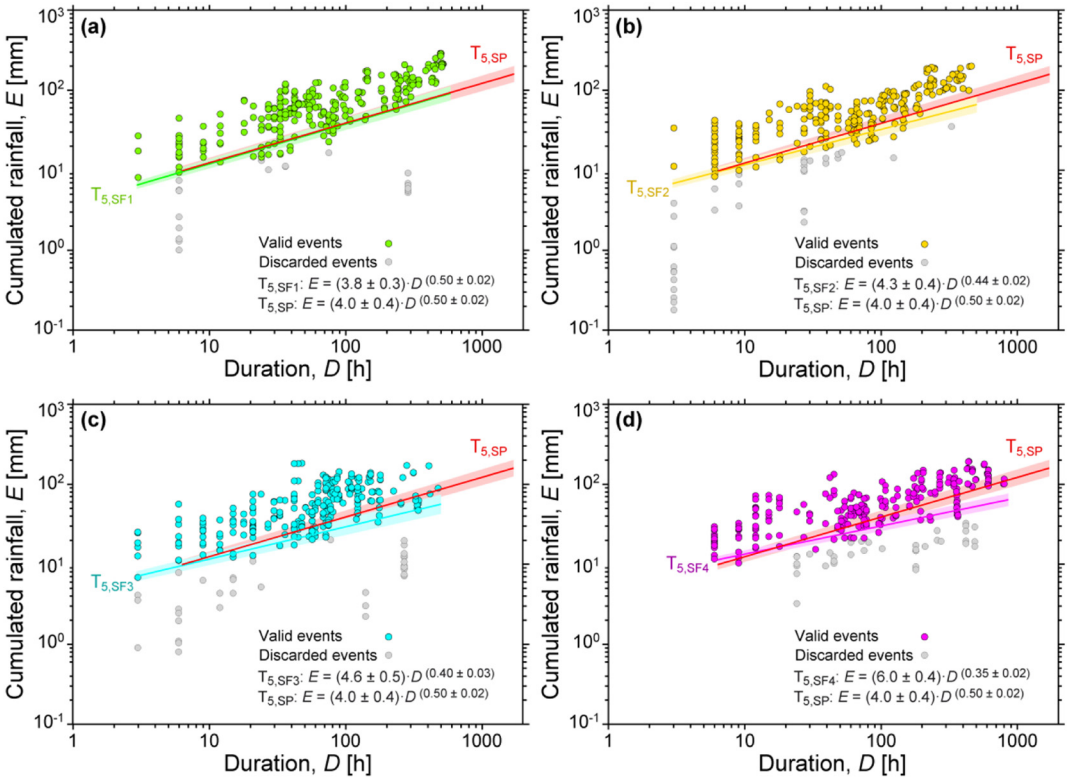

Fig. 8. Cumulated event rainfall E (mm) vs. rainfall duration D (h) conditions that have generated the largest number of unstable cells in the simulated events for the S_{F1} (green dots in (a)), the S_{F2} (yellow dots in (b)), the S_{F3} (cyan dots in (c)) and S_{F4} (red dots in (d)) data sets. Grey dots show rainfall conditions unlikely responsible for failures in the area. Colored curves are the corresponding 5% thresholds $T_{5,SF1}$ (a), $T_{5,SF2}$ (b), $T_{5,SF3}$ (c) and $T_{5,SF4}$ (d). Shaded areas show the statistical uncertainty associated to the new thresholds (cf. Section 5.4). (For interpretation of the references to colour in this figure legend, the reader is referred to the web version of this article.) (For interpretation of the references to colour in this figure legend, the reader is referred to the web version of this article.)

change in response to the projected climate changes, though the conclusion is drawn from results with large statistical uncertainty.

5. Discussion

The general modelling framework commonly adopted by impact studies to investigate the consequences of the projected climate and environmental changes on the stability of slopes, and on the projected changes in landslide hazard, consists of two main modelling chains (Gariano and Guzzetti, 2016). The first chain links the output of an ensemble of GCMs for established emissions scenarios to regional climate models, which may be further bias-corrected and downscaled adopting different procedures. The climate-related modelling chain, including a bias correction step, was formulated in general terms in Rianna et al. (2014) as well. The output of the first chain is then used as an input to the second chain that consists of slope stability models engineered to assess the stability conditions of single slopes or entire catchments, based on the local geo-hydrological and environmental settings. Typically, the two modelling chains are first calibrated or validated on past climate, geo-hydrological and environmental data. Next, the calibrated models are applied to future climate projections, to obtain future landslide projections.

Fig. 10 shows a graphical representation of the modelling scheme adopted in this study, which falls in the general modelling framework described above, with adjustments and some novelty. Our implementation of the climate evaluation chain included gridded downscaled precipitation data obtained using the RainFARM stochastic downscaling technique (Rebora et al., 2006a, 2006b; D'Onofrio et al., 2014), applied to the output of a RCM (WRF; Pieri et al. (2015)). We then sampled downscaled data at the locations of 56 existing rain gauges in our study area (Fig. 1), for which measured rainfall records were available. This allowed to analyze the downscaled, synthetic rainfall data at the same locations of the measured rainfall data. Our implementation of the slope stability chain relied on TRIGRS v. 2.1 (Alvioli and Baum, 2016), a recent parallel implementation of the TRIGRS v. 2.0 for the timing and spatial distribution of rainfall-induced shallow landslides (Baum et al., 2008).

Table 2
Statistics for the results of the slope stability simulations performed by TRIGRS v. 2.1 (Alvioli and Baum, 2016), in terms of the number ($\#L$) and the area (A_L) of the modelled landslides. Minimum number of landslides is zero, when no grid cells in a simulation have FS < 1. Smallest landslide has area $A_L = 10\ m \times 10\ m = 100\ m^2$, by construction.

ID	Period	$\#L_{max}$	$\#L_{avg}$	$A_{L,max}$ [m^2]	$A_{L,avg}$ [m^2]
M	2003–2011	63,897	1277	34,010	723
S_P	2002–2015	37,596	751	23,507	529
S_{F1}	2010–2019	39,860	797	19,311	604
S_{F2}	2020–2029	29,187	583	31,909	405
S_{F3}	2030–2039	32,915	658	15,709	518
S_{F4}	2040–2049	28,409	568	15,704	413

5.1. Rainfall events

The first novelty of our work consisted in selecting rainfall events, R_E from the available rainfall series, and to use them to force the spatially-distributed, time-varying slope stability modelling (Result 1 in Fig. 10). Rainfall events are (nearly) continuous periods of rain separated by a dry period (Guo, 2002; Guzzetti et al., 2007; Brunetti et al., 2010; Saito et al., 2010; Shamsudin et al., 2010; Melillo et al., 2015, 2016), and are known to be a better proxy of the rainfall conditions responsible for the initiation of landslides than other fixed-length measures of the rainfall duration, including hours or days (Aleotti, 2004; Guzzetti et al., 2007; Brunetti et al., 2010; Berti et al., 2012). For this reason, we maintain that extraction of R_E from the measured (M) and the synthetic (S_P

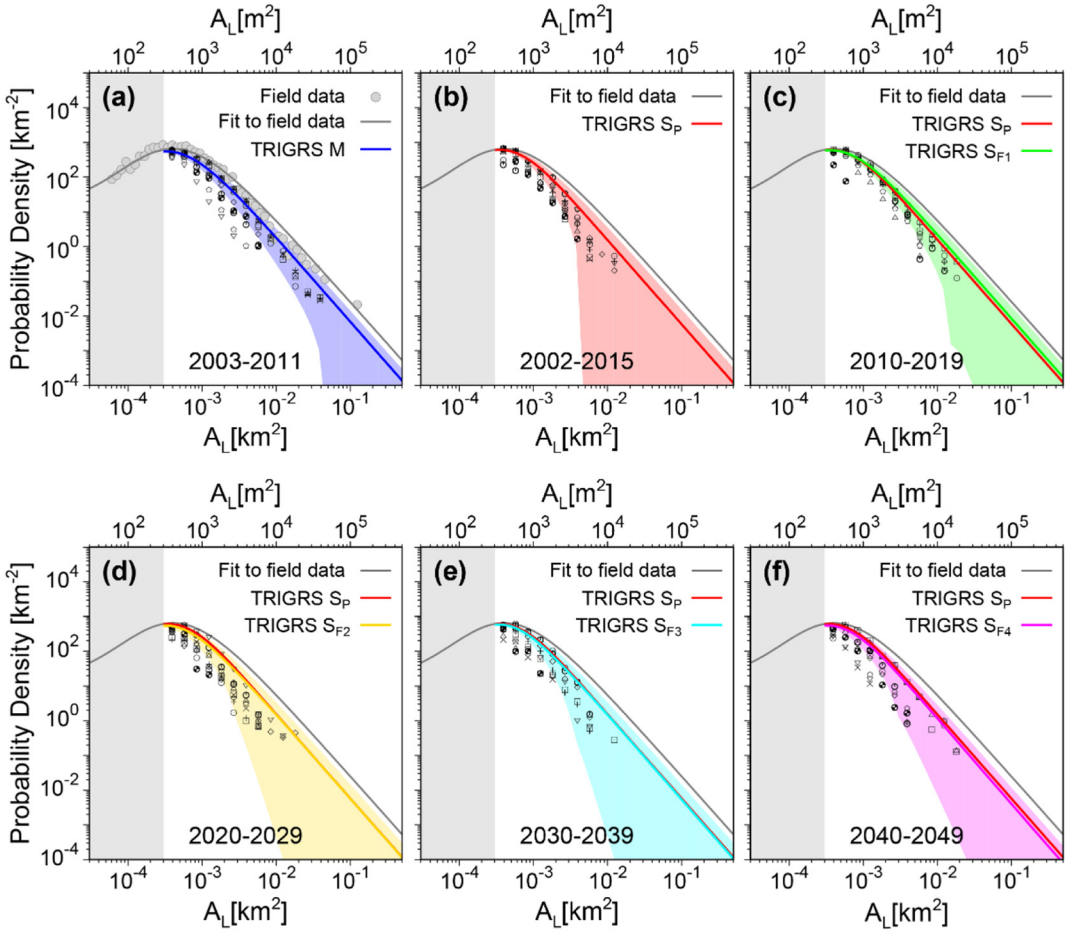

Fig. 9. Dependence of landslide probability density on landslide area, A_L (m^2, in the upper x-axis, and km^2, in the lower x-axis) determined for each landslide as the sum of all adjacent unstable grid cells i.e., cell that have FS < 1 (Alvioli et al., 2014). TRIGRS simulations for the six data sets described in this work (a-f). Curves in colors are fits to TRIGRS results with the function in Eq. (a2), by fitting results from individual events and averaging over individual results; their limit of validity is outside of the shaded area. Symbols show a sample subset of the results from 10 events out of the total 50 events for each data set; different symbols were used for different events. Discarded points are not shown.

and S_F) rainfall series, and the subsequent identification of the rainfall events that have resulted in modelled landslides, is a meaningful, well-founded procedure to determine the influence of changing rainfall patterns on slope stability conditions, and their possible variations in response to the projected climate changes.

Our results showed that the downscaled rainfall time series obtained using the RainFARM stochastic technique can be used to obtain synthetic rainfall events, adopting the same algorithm proposed by Melillo et al. (2015, 2016) for the automatic selection of the rainfall events from standard rainfall records. The event selection algorithm acts as a filter on the rainfall series, which in general are quite different (see e.g. Fig. 2). As a result of the filtering, rainfall events from both the measured and the synthetic series become very similar (see e.g. Fig. 3).

The ECDFs of the R_E duration, D and the cumulated event rainfall, E for the measured (M, blue in Fig. 3) and the synthetic past (S_P, red in Fig. 3) R_E are very similar, with the S_P events slightly longer, therefore totalling a slightly larger cumulated rainfall than the M events. The differences between the ECDFs are sufficiently small to allow for a meaningful comparison of the spatially distributed, time-varying slope stability models forced by the measured and the synthetic rainfall series. Also, the S_P events exhibit a larger variability than the M events, as shown by the larger extent of the red shaded areas in Fig. 3, compared to the blue shaded areas. Comparison of the ECDFs for the synthetic past events (S_P) and the synthetic future events for the four considered decadal periods (S_{F1}, S_{F2}, S_{F3}, S_{F4}) reveals that the ECDFs are nearly identical (Fig. 4), indicating that the S_F rainfall events are similar to the measured R_E. Hence, the slope stability simulations obtained using the synthetic R_E can be compared consistently with each other, and with simulations performed using the measured rainfall events.

5.2. Rainfall thresholds and area of landslides

The second novelty of the work (Result 2 in Fig. 10) consists in the method used to compare the effects of the rainfall events forcing on the slope stability conditions modelled by TRIGRS v. 2.1 (Alvioli and Baum, 2016), for the different considered periods. We based the comparison on the analysis of (i) the rainfall thresholds that have resulted in (modelled) landslides, and (ii) the modelled probability density of landslide area, $P(A_L)$.

Analysis of Fig. 7 reveals that the $T_{5,M}$ thresholds defined for the 50 rainfall events with modelled landslides in the period 2003–2011 (M), and for the 50 synthetic past rainfall events with modelled landslides in the partially overlapping period 2002–2015 (S_P) are nearly identical, with the main difference that the $T_{5,M}$ threshold is valid in the range $3 \le D \le 939$ h (40 days), whereas the $T_{5,SP}$ threshold is valid in the longer range $6 \le D \le 1600$ h (66 days). This is a result of the different duration of the R_E in the M and S_P periods (Table 1). Despite the difference, we maintain that the $T_{5,M}$ threshold is valid for the S_P events in their full rainfall duration range, and vice versa the $T_{5,SP}$ threshold is valid for the M events in their full duration range.

Analysis of Fig. 8 reveals that $T_{5,F1}$ is correctly equivalent to the $T_{5,SP}$ threshold, as they are obtained from synthetic data partially overlapping in time. The $T_{5,F2}$, $T_{5,F3}$, and $T_{5,F4}$ thresholds defined for the next three future non-overlapping decadal periods are not similar to the $T_{5,}$

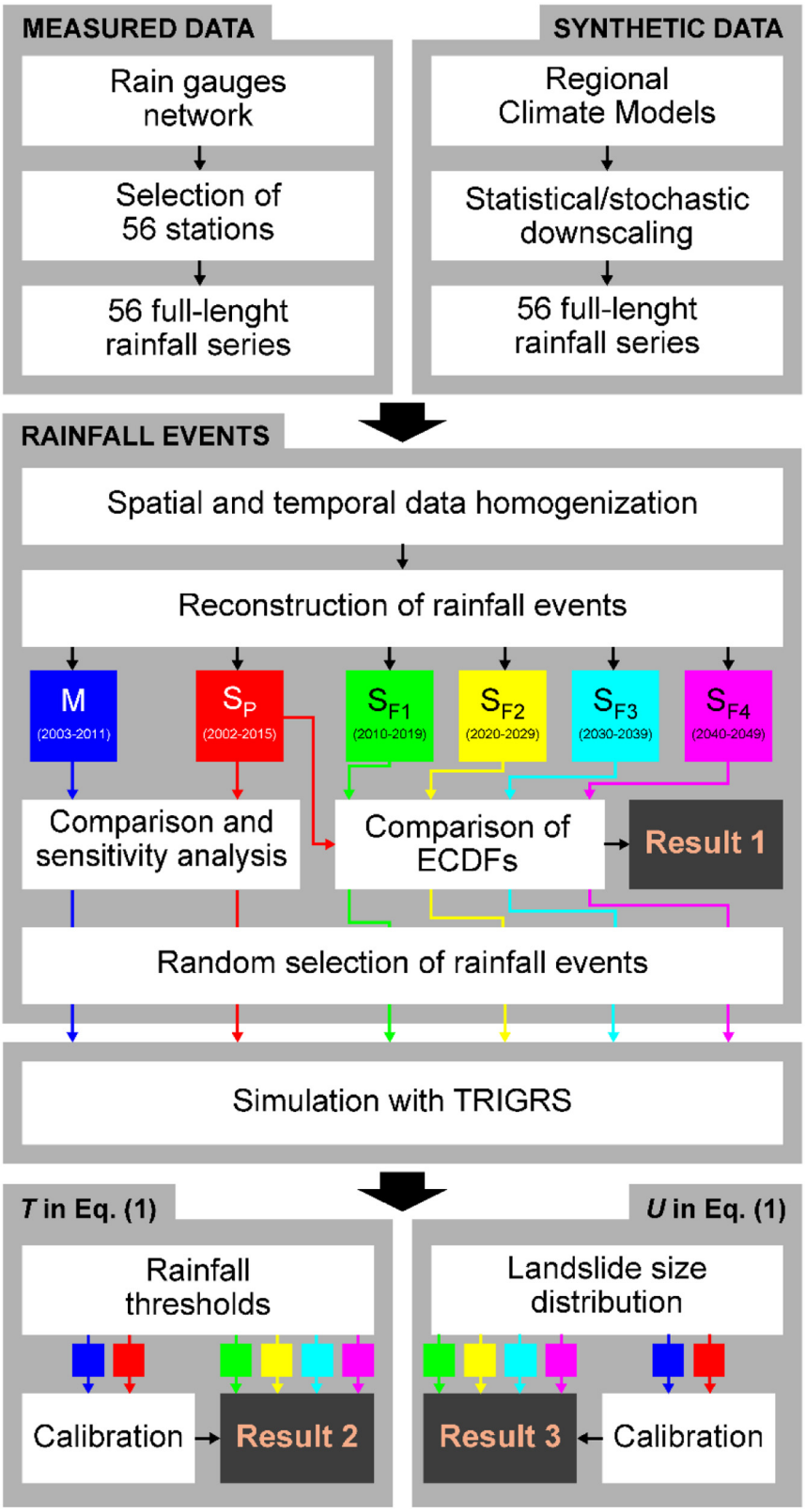

Fig. 10. Modelling framework exemplifying the different steps performed in this study. Result 1: R_E can be extracted the stochastically-downscaled rainfall fields obtained using the modified RainFARM technique, similarly to the measured rainfall data, and used meaningfully in numerical slope stability simulations. Result 2: the (*D*,*E*) rainfall conditions that can result in (modelled) landslides are projected to change in the future period 2010–2049. Result 3: the area distribution of landslides is not expected to change in the future in the study area, in the same future period.

$_{SP}$ threshold, even considering the uncertainty associated to the thresholds for the different periods. We conclude that the projected changes in precipitation patterns are expected to vary the minimum cumulated rainfall, for different durations, necessary to initiate landslides in our study area. We further observe that the $T_{5,F1}$, $T_{5,F2}$, $T_{5,F3}$, and $T_{5,F4}$ are progressively less steep in the *DE* plane. A horizontal threshold implies

that landslides are initiated when a fixed cumulated rainfall E is exceeded, independently of the rainfall duration D (Guzzetti et al., 2007, 2008a, 2008b). The finding that future thresholds in the study area will progressively depend more on the cumulated rainfall is in agreement with the projected increase of more intense and frequent rainfall events (IPCC, 2014) in several regions, including the European area as shown by CORDEX models (Fisher and Knutti, 2016).

Analysis of Fig. 9 reveals that the probability density of landslide area, $P(A_L)$ obtained for the modelled landslides initiated by the measured (M, observed) rainfall events is very similar to the $P(A_L)$ determined by Malamud et al. (2004) for mapped event landslides also in the same general geographical area (Result 3 in Fig. 10). The modelled $P(A_L)$ has the same slope as the empirical one, albeit it is slightly lower than the empirical $P(A_L)$. Further analysis of Fig. 9 reveals (i) the main difference between the M and S_P results is the increased uncertainty in the latter, and (ii) that the modelled landslides initiated by the synthetic rainfall events for different future periods exhibit the same $P(A_L)$ as the one obtained from the S_P events, with comparable (large) uncertainty. We conclude that the area distribution of landslides is not expected to change in the future, in our study area. We acknowledge that the large statistical uncertainty of the calculated $P(A_L)$ distributions makes the results less robust than for the rainfall thresholds.

We note that TRIGRS models the timing and spatial distribution of shallow landslides (Baum et al., 2008; Alvioli and Baum, 2016), and is not suited for the modelling of large, deep-seated landslides, which are abundant in the area (Cardinali et al., 2001; Guzzetti et al., 2008a). We acknowledge that uncertainty remains in the (E, D) rainfall conditions and the corresponding thresholds for the initiation of large, deep-seated landslides in the study area.

5.3. Projected landslide hazard changes

When examining the complex results of the spatially distributed, time-varying slope stability modelling (a total of 1800 simulations, each consisting of a number of pixels varying between 270,000 for the smaller sub-area, A1 in Figs. 1, and 1,050,000 for the larger sub-area, A2 in Fig. 1), we faced the problem of finding a single, compact measure to express the expected changes in the stability conditions of the slopes in our study area, in response to the projected climate changes. For the purpose, we selected landslide hazard, H (Guzzetti et al., 2005), which we define in its most general form as:

$$H(v,t) = \quad T(v,t)U(v,t)S(v,t), \tag{1}$$

where T, U and S are three functions, described in the following, v is a set of environmental conditions (and related variables) relevant to the occurrence of landslides, and t is time.

Here, we examine the effects of the variations (or lack of variations) of the rainfall thresholds and of the probability density of landslide area, $P(A_L)$ on landslide hazard, $H(v, t)$.

In Eq. (1), $T(v, t)$ is the hazard's explicit time dependence i.e., the expected frequency of landslide events, or the average return period between successive landslide events (Guzzetti et al., 2005). To evaluate the possible variation in the temporal probability of landslide occurrence, we examine the rainfall thresholds, and their variations (Figs. 7, 8). Lower (higher) rainfall thresholds in a period, correspond to a higher (lower) expected frequency of landslide events and to a shorter (longer) average return period between successive landslide events, compared to other periods. Considering the small uncertainty associated to the thresholds, and the evidence that the thresholds vary significantly in the considered future periods (S_{F1}, S_{F2}, S_{F3}, S_{F4}) with respect to the past periods (M, S_P), we conclude that the temporal component of landslide hazard, $T(v, t)$ is projected to vary. Developing an explicit functional form of $T(v, t)$ would require information about the exceedance probability for landslide occurrence as a function of time (Coe et al., 2000; Crovelli, 2000; Roberds, 2005; Rossi et al., 2010; Witt et al., 2010), and is beyond the scope if this work.

$U(v, t)$ measures landslide magnitude. Following Guzzetti et al. (2005), here we use landslide area A_L, as a proxy for $U(v, t)$, and we take the (possible) changes in the probability density of landslide area, $P(A_L)$ as a proxy for the (possible) variations in $U(v, t)$. We note here that a steeper (less steep) probability density curve indicates a larger (smaller) proportion of small landslides, as compared to large landslides. We found no substantial variation of $P(A_L)$ calculated for the future periods with respect to the past (Fig. 9). We conclude that we do not expect variations in the landslide magnitude in the study area within our modelling chain, though statistical uncertainty is large in this case.

In Eq. (1), $S(v, t)$ is landslide susceptibility, the spatial component of H that measures the likelihood of spatial landslide occurrence, given a set of environmental conditions (Guzzetti et al., 2005). Here we do not consider landslide susceptibility and its possible variations due to the projected climate changes. We stress here that landslide susceptibility depends on factors that are not expected to change in the time-frame of our analyses, including e.g., morphology, lithology, and on other factors that may – and probably will – change in the considered time-frame due to climate variations, including e.g., land use and land cover (Guzzetti et al., 2005; Gariano and Guzzetti, 2016; Gariano et al., 2017a).

We conclude that, even if landslide susceptibility $S(v, t)$ remains the same in our study area in the considered period, landslide hazard, $H(v, t)$ is expected to change because, albeit the probability density of landslide area $P(A_L)$, a proxy for the magnitude component $U(v, t)$ of landslide hazard, is not expected to vary, the rainfall thresholds for the initiation of landslides, and hence the temporal component $T(v, t)$ of landslide hazard, is projected to change.

We note that our results are different from the conclusions of Ciabatta et al. (2016), who investigated the impact of climate change on landslide occurrence in Umbria, Central Italy, using rainfall and temperature fields downscaled from GCM model outputs for the past period 1990–2013, and for the two future periods 2040–2069 and 2070–2099. These authors predicted an increase of up to >40% in landslide events in Umbria. We stress that the results obtained by the two studies are not directly comparable, because of the different climate projections used, the different period covered, and the different quantities used to determine the predicted landslide occurrence.

5.4. Uncertainty

Our modelling chain is undoubtedly affected by uncertainties, which have different origins and meanings, in the different modelling steps (Fig. 10).

At the top of the modelling chain, different possible future scenarios could have been used, leading to a corresponding uncertainty in the projections. In the literature a few works exist about the analysis of uncertainties related to the selection of climate projections (Hawkins and Sutton, 2009; Mendlik and Gobiet, 2016; Wilcke and Bärring, 2016), the role of bias correction in impact studies (Teutschbein and Seibert, 2012; Maraun, 2016; Ehret et al., 2012) and the challenges posed by the use of multi-model ensemble simulations (Knutti et al., 2010). Furthermore, climate models differ in terms of parameterizations included, resolution and processes which they represent, again leading to an important source of uncertainty. Different GCMs may be used to provide external boundary conditions for the RCMs providing a further source of model uncertainty. In order to streamline our analysis, in this work we considered only the case where a single model run and a single future scenario are used, but the impact of these sources of uncertainty should be evaluated.

The uncertainty associated to the event rainfall duration D, and the event cumulated rainfall E, calculated for the measured (M) and the synthetic past (S_P) events shown in Fig. 3 is statistical, and measures the variability of the two rainfall event metrics in each period. The

uncertainty shown in Fig. 5 is related to the large number of random selections performed to obtain the average ECDFs selected to represent each set. We did not attempt to propagate the uncertainty associated to the rainfall metrics originated in the climate modelling chain onto the single R_E, or the slope stability modelling. We maintain that this is – at least partially – justified by the smoothing of the uncertainties operated by the event selection procedure.

The uncertainty associated with the rainfall thresholds shown in Fig. 7 depends on the number and the distribution of the (D, E) conditions that represent the rainfall events, and on the statistical method used to define the thresholds (Melillo et al., 2015, 2016). Similarly, the uncertainty in the probability density of landslide area, $P(A_L)$ shown in Fig. 9 depends on the number and the distribution of the empirical data points, and on the statistical method used to define $P(A_L)$. The latter two uncertainties do not bear any direct physical relation to the original climate model uncertainties.

5.5. Model applicability

In this work, we adopted a rather complex modelling chain (Fig. 10) that included components for (i) the downscaling of the precipitation fields (Rebora et al., 2006a, 2006b; D'Onofrio et al., 2014), (ii) the selection of rainfall events (Melillo et al., 2015, 2016), (iii) the definition of *ED* rainfall thresholds (Brunetti et al., 2010; Peruccacci et al., 2012), and for (iv) the spatially distributed, time-varying slope stability assessment (Alvioli and Baum, 2016). Further, we joined the different models using a number of assumptions and approximations.

The RainFARM technique is implemented in an easy-to-use software package currently available in GitHub.[1] It may suffer from computer memory limitations in case precipitation fields over large areas have to be downscaled at extremely high resolution. In the present study a machine with 48GB of memory was used. Downscaled data corresponding to 40 years for the study area occupies 4GB on disk.

The R_E selection algorithm (Melillo et al., 2015, 2016; available at CNR-IRPI[2]) proved robust, and the implementation software did not suffer from computer storage or processing limitations. Similar considerations hold for the definition of the rainfall thresholds. The method proposed by Brunetti et al. (2010) and Peruccacci et al. (2012) performed well on both the measured and the synthetic data sets, and the implementation software did not suffer from computer limitations. We further note that the R_E selection procedure needs to be run only once, since the R_E do not vary, and that the rainfall thresholds are univocally defined once the rainfall conditions responsible for landslide occurrence are identified.

On the other hand, the TRIGRS model, or any other similar physically based numerical model (e.g., Montgomery and Dietrich, 1994; Burton and Bathurst, 1998; Malet et al., 2005; Rigon et al., 2006; Simoni et al., 2008; Anagnostopoulos and Burlando, 2012; Von Ruette et al., 2013; Mergili et al., 2014), has inherent computer storage and processing limitations that impose careful selection of an appropriate modelling strategy. Parallelization of the existing TRIGRS code (Alvioli and Baum, 2016; available in GitHub[3]) was a first step, but further efforts are needed to produce physically-based models for the timing and spatial distribution of rainfall-induced shallow landslides that can be used efficiently for climate impact studies.

6. Conclusions

We investigated the causal relationships between downscaled climate projections and slope stability conditions in a 422 km^2 area in the Upper Tiber River Basin, Central Italy, where post-orogenic sediments of continental origin crop out (Fig. 1) and landslides are abundant (Cardinali et al., 2001; Guzzetti et al., 2008a).

The main results of this work can be summarized as follows:

- We showed that spatially distributed rainfall fields obtained by applying the RainFARM stochastic downscaling technique to data from the WRF regional climate model can be treated by the algorithm and the implementation software proposed by Melillo et al. (2015, 2016) for the automatic detection of rainfall events that have triggered landslides from rainfall series.
- In our study area, comparison of the empirical cumulative density functions (ECDFs) for 56 measured (observed) rainfall records, and for an equal number of synthetic (projected) rainfall series at the same locations (Fig. 3), revealed that the differences were sufficiently small as compared to the differences in MAP (Fig. 2) to allow for a meaningful comparison of the spatially distributed, time-varying slope stability model TRIGRS v. 2.1 (Alvioli and Baum, 2016) forced by the measured and the synthetic rainfall data.
- We showed that 5% non-exceedance probability, empirical cumulated event rainfall – rainfall duration (*ED*) thresholds for the possible occurrence of landslides (Brunetti et al., 2010; Peruccacci et al., 2012) obtained using the results of 1800 spatially distributed, time-varying slope stability simulations forced with observed (measured) and projected (synthetic) rainfall series, vary with time in our study area. We conclude that the (D, E) rainfall conditions that can result in (modelled) landslides are projected to change in the future period 2010–2049. We also showed that thresholds for future events will depend more on the cumulated rainfall than on the rainfall duration than they currently do.
- We further showed that the probability density functions of landslide areas, $P(A_L)$ derived from the same sets of spatially distributed, time-varying slope stability simulations were all rather similar, though with large statistical uncertainty. We therefore infer that the area distribution of landslides is not expected to change in the future in the study area.
- Lastly, adopting a general and widely accepted definition for landslide hazard (Guzzetti et al., 2005), we showed that landslide hazard is expected to change in the study area, because the rainfall thresholds for the initiation of landslides are projected to change.

This work presents for the first time the application of a modelling chain, in which high-resolution rainfall fields, obtained with a stochastic downscaling technique, applied to rainfall climate projections from a Regional Climate Model, are used to drive spatially-distributed, time-varying slope stability models, using physically-based, deterministic approaches. Our results open the floor for other future similar applications in which RCM and GCM outputs are downscaled and used for the assessment of the impacts on slope stability of projected climate changes.

Acknowledgments

Work partially supported by the Italian National Department for Civil Protection (DPC). Rainfall data were provided by DPC and are not accessible to the public. M.A. acknowledges the CINECA award GEOMORPH2 under the ISCRA initiative for the availability of high performance computing resources and support. E.P. and J.v.H. acknowledge support by the the Project of Interest "NextData" of the Italian Ministry for Education, University and Research.

Appendix A

In this appendix, we provide further details on two key steps of our modelling chain (Fig. 10).

[1] https://github.com/jhardenberg/RainFARM.jl
[2] http://geomorphology.irpi.cnr.it/tools/rainfall-events-and-landslides-thresholds
[3] https://github.com/baum-usgs/landslides-trigrs

6.1. Rainfall thresholds

The definition of rainfall thresholds from the pairs of (D, E) rainfall conditions that have resulted in (modelled) landslides in the TRIGRS outputs required some calibration. We first observed that a few landslide-triggering rainfall conditions, resulting from a very few (hundreds, out of hundreds of thousands) grid cells with $F_S < 1.0$, exhibited a short duration ($D < 9$ h) and a corresponding low cumulated rainfall ($E < 10$ mm). Inspection of these (D, E) rainfall pairs revealed that they were below, or well below the empirical $T_{5,AMU}$ threshold valid for the study area (Peruccacci et al., 2012). We considered these rainfall conditions not representative of overt slope instability conditions. To discard the non-representative rainfall pairs, we selected a cutting line parallel to $T_{5,AMU}$: (D, E) points lying below the cutting line will be discarded, and points above the line will be considered as representative of the rainfall conditions capable of triggering landslides in the area. We adjusted the position of the cutting line by calculating a $T_{5,M}$ threshold with only the representative rainfall pairs, and then selecting the particular cutting line that resulted in the best agreement between the $T_{5,M}$ and the $T_{5,AMU}$ thresholds. We performed the calibration (i.e., the selection of position of the cutting line) using rainfall conditions of the observed data set (M), and we adopted the same cutting line to determine thresholds for the (past and future) synthetic rainfall data sets (S_P and S_F). The curves $T_{5,M}$ and $T_{5,SP}$ shown in Fig. 7, and the curves $T_{5,SF1}$, $T_{5,SF2}$, $T_{5,SF3}$ and $T_{5,SF4}$ show in Fig. 8, were calculated using the valid (D, E) rainfall conditions.

6.2. Landslide area

The output of the TRIGRS simulations was used to model the distribution of landslide areas. From the pixel-based output produced by TRIGRS, we singled out individual landslides, where a "landslide" was as a cluster of adjacent unstable cells with FS < 1.0. For each landslide, we then computed the landslide area A_L, summing the area of all the adjacent 10 m × 10 m grid cells forming the landslide. Physically based models are known to produce unrealistically small, one-pixel-size unstable (stable) areas, whose $P(A_L)$, remarkably, follow power law distributions; whereas $P(A_L)$ distributions of real event landslides are known to have a maximum (the "rollover"). Fitting the $P(A_L)$ obtained from TRIGRS with a power law (a straight line in log-log coordinates) would hinder the true structure of the data, and will likely produce an erroneous result. To cope with the problem, we devised the following procedure.

Landslide area distributions are often presented in the form of probability density functions, parameterized e.g., by an inverse Gamma function (Malamud et al., 2004),

$$P(A_L) = \frac{1}{a\Gamma(\rho)} \left(\frac{a}{A_L - s}\right)^{\rho+1} \exp\left(-\frac{a}{A_L - s}\right), \quad \text{(a1)}$$

where, $\Gamma(\rho)$ is the Gamma function of ρ, a parameter controlling the power-law decay for medium and large landslide areas, a primarily controls the location of the maximum probability distribution (the "rollover"), and s primarily controls the exponential decay for small landslide areas.

In the TRIGRS results, we assumed as unrealistic all the (modelled) landslides with a very small A_L (the small-A_L part of the distribution), constituted primarily by a single grid cell or a very few grid cells, and we disregarded all the very small landslides up to a threshold value of A_L dictated by the requirement of observing a rollover-like behavior in the remaining data, for the measured (M) data set. We complemented the remaining data with fictitious data points sampled from the small-A_L part of the distribution of Eq. (a1) with values of the a, s, ρ parameters fitted to real landslide data. We fitted the resulting data with the same functional form of Eq. (a1), but with a larger set of parameters, in order to be able to fit the power-law part of the distributions while keeping almost fixed the small-A_L part of the curve. The new parametrization is as follows:

$$P(A_L) = \frac{1}{a_1\Gamma(\rho_1)} \left(\frac{a_2}{A_L - s_1}\right)^{\rho_2+1} \exp\left(-\frac{a_3}{A_L - s_2}\right), \quad \text{(a2)}$$

where the new parameters are a_1, a_2, a_3, s_1, s_2, ρ_1 and ρ_2. This step is a calibration to the simulations obtained with observed data. We then used the same value of the cut, $A_L = 300$ m^2, for all the synthetic data sets. It is understood that the small-A_L part of the resulting curve is meaningless, thus it is not shown in Fig. 9. The procedure was repeated for each of the 50 events in each of the six data sets, resulting in 50 sets of values of the a_1, a_2, a_3, s_1, s_2, ρ_1 and ρ_2 parameters appearing in Eq. (a2). The envelope of the corresponding 50 curves is shown in Fig. 9 with a shaded area, for each of the six different data sets. Discarded points, with $A_L < 300$ m^2, are not shown in the Figure. Our final results, shown in Fig. 9 with solid curves in colour, were obtained by plotting Eq. (a2) with the average value of each of the parameters.

Appendix B. Supplementary data

Supplementary data to this article can be found online at https://doi.org/10.1016/j.scitotenv.2018.02.315.

References

Aleotti, P., 2004. A warning system for rainfall-induced shallow failures. Eng. Geol. 73: 247–265. https://doi.org/10.1016/j.enggeo.2004.01.007.

Alvioli, M., Baum, R.L., 2016. Parallelization of the TRIGRS model for rainfall-induced landslides using the message passing interface. Environ. Model. Softw. 81:122–135. https://doi.org/10.1016/j.envsoft.2016.04.002.

Alvioli, M., Guzzetti, F., Rossi, M., 2014. Scaling properties of rainfall-induced landslides predicted by a physically based model. Geomorphology 213:38–47. https://doi.org/10.1016/j.geomorph.2013.12.039.

Anagnostopoulos, G.G., Burlando, P., 2012. An object-oriented computational framework for the simulation of variably saturated flow in soils, using a reduced complexity model. Environ. Model. Softw. 38:191–202. https://doi.org/10.1016/j.envsoft.2012.06.002.

Badas, M.G., Deidda, R., Piga, E., 2005. Orographic influences in rainfall downscaling. Adv. Geosci. 2, 285–292 (SRef-ID: 1680-7359/adgeo/2005-2-285).

Baum, R., Savage, W., Godt, J.W., 2008. TRIGRS — a FORTRAN program for transient rainfall infiltration and grid-based regional slope-stability analysis, version 2.0. U.S. geological survey open-file report 2008-1159 (75 pp.). https://pubs.usgs.gov/of/2008/1159.

Bellugi, D., Milledge, D.G., Dietrich, W.E., McKean, J.A., Perron, J.T., Sudderth, E.B., Kazian, B., 2015. A spectral clustering search algorithm for predicting shallow landslide size and location. J. Geophys. Res. Earth Surf. 120:300–324. https://doi.org/10.1002/2014JF003137.

Berti, M., Martina, M.L.V., Franceschini, S., Pignone, S., Simoni, A., Pizziolo, M., 2012. Probabilistic rainfall thresholds for landslide occurrence using a Bayesian approach. J. Geophys. Res. 117, F04006. https://doi.org/10.1029/2012JF002367.

Bordoy, R., Burlando, P., 2014. Stochastic downscaling of climate model precipitation outputs in orographically complex regions: 2. Downscaling methodology. Water Resour. Res. 50:562–579. https://doi.org/10.1002/wrcr.20443.

Brunetti, M.T., Peruccacci, S., Rossi, M., Luciani, S., Valigi, D., Guzzetti, F., 2010. Rainfall thresholds for the possible occurrence of landslides in Italy. Nat. Hazards Earth Syst. Sci. 10:447–458. https://doi.org/10.5194/nhess-10-447-2010.

Brussolo, E., von Hardenberg, J., Ferraris, L., Rebora, N., Provenzale, A., 2008. Verification of quantitative precipitation forecasts via stochastic downscaling. J. Hydrometeorol. 9: 1084–1094. https://doi.org/10.1175/2008JHM994.1.

Burton, A., Bathurst, J., 1998. Physically based modelling of shallow landslide sediment yield at a catchment scale. Environ. Geol. 35 (2–3):49–99. https://doi.org/10.1007/s002540050296.

Cardinali, M., Antonini, G., Reichenbach, P., Guzzetti, F. (2001). Photo-geological and landslide inventory map for the Upper Tiber River basin. CNR, Gruppo Nazionale per la Difesa dalle Catastrofi Idrogeologiche, Publication n. 2154, scale 1: 100,000. (Available for download at): http://maps.irpi.cnr.it/website/tevere/tevere_start.htm

Ciabatta, L., Camici, S., Brocca, L., Ponziani, F., Stelluti, M., Berni, N., Moramarco, T., 2016. Assessing the impact of climate-change scenarios on landslide occurrence in Umbria region, Italy. J. Hydrol. 541:285–295. https://doi.org/10.1016/j.jhydrol.2016.02.007.

Ciccarelli, N., von Hardenberg, J.A., Ronchi, C., Vargiu, A., Pelosini, R., 2008. Climate variability in north-western Italy during the second half of the 20th century. Glob. Planet. Chang. 63:185–195. https://doi.org/10.1016/j.gloplacha.2008.03.006.

Ciervo, F., Rianna, G., Mercogliano, P., Papa, M.N., 2017. Effects of climate change on shallow landslides in a small coastal catchment in southern Italy. Landslides 14 (3): 1043–1055. https://doi.org/10.1007/s10346-016-0743-1.

Coe, J.A., 2016. Landslide Hazards and Climate Change: A Perspective from the United States. In: Slope Safety Preparedness for Impact of Climate Change. In: Ho, K., Lacasse, S., Picarelli, L. (Eds.), Taylor & Francis Group, Boca Raton. CRC Press, FL USA:pp. 479–523 https://doi.org/10.1201/9781315387789-16.

Coe, J.A., Godt, J., 2012. Review of approaches for assessing the impact of climate change on landslide hazards. In: Eberhardt, E., Froese, C., Turner, A.K., Leroueil, S. (Eds.), Landslides and engineered slopes, protecting society through improved understanding: proceedings of the 11th international and 2nd north American symposium on landslides and engineered slopes, Banff, Canada, 3-8 June, Taylor & Francis Group, London. 1 :pp. 371–377. https://pubs.er.usgs.gov/publication/70006359.

Coe, J.A., Michael, J.A., Crovelli, R.A., Savage, W.Z., 2000. Preliminary Map Showing Landslide Densities, Mean Recurrence Intervals, and Exceedance Probabilities as Determined from Historic Records, Seattle, Washington. US Geological Survey Open-File Report 00–303. US Geological Survey, Reston, VA https://pubs.usgs.gov/of/2000/ofr-00-0303.

Corominas, J. (2000). Landslides and climate. Keynote lecture. In: Proceedings of the 8th International Symposium on Landslides, Bromhead, E., Dixon, N., Ibsen, M.L. (Eds.), A. A. Balkema, Cardiff, 4, 1–33.

Crovelli, R.A., 2000. Probability models for estimation of number and costs of landslides. U.S. Geological Survey Open File Report OO-249 (23p). https://pubs.usgs.gov/of/2000/ofr-00-0249.

Diffenbaugh, N.S., Field, C., 2013. Changes in ecologically critical terrestrial climate conditions. Science 341 (6145):486–492. https://doi.org/10.1126/science.1237123.

D'Onofrio, D., Palazzi, E., von Hardenberg, J., Provenzale, A., Calmanti, S., 2014. Stochastic rainfall downscaling of climate models. J. Hydrometeorol. 15:830–843. https://doi.org/10.1175/JHM-D-13-096.1.

Ehret, U., Zehe, E., Wulfmeyer, V., Warrach-Sagi, K., Liebert, J., 2012. HESS opinions "should we apply bias correction to global and regional climate model data?". Hydrol. Earth Syst. Sci. 16 (9):391. https://doi.org/10.5194/hess-16-3391-2012.

Fisher, E.M., Knutti, R., 2016. Observed heavy precipitation increase confirms theory and early models. Nat. Clim. Chang. 6:986–991. https://doi.org/10.1038/nclimate3110.

Gabellani, S., Boni, G., Ferraris, L., von Hardenberg, J., Provenzale, A., 2007. Propagation of uncertainty from rainfall to runoff: a case study with a stochastic rainfall generator. Adv. Water Resour. 30:2061–2071. https://doi.org/10.1016/j.advwatres.2006.11.015.

Gariano, S.L., Guzzetti, F., 2016. Landslides in a changing climate. Earth Sci. Rev. 162: 227–252. https://doi.org/10.1016/j.earscirev.2016.08.011.

Gariano, S.L., Petrucci, O., Rianna, G., Santini, M., Guzzetti, F., 2017a. Impacts of past and future land changes on landslides in southern Italy. Reg. Environ. Chang. https://doi.org/10.1007/s10113-017-1210-9.

Gariano, S.L., Rianna, G., Petrucci, O., Guzzetti, F., 2017b. Assessing future changes in the occurrence of rainfall-induced landslides at a regional scale. Sci. Total Environ. 15 (596–597):417–426. https://doi.org/10.1016/j.scitotenv.2017.03.103.

Giorgi, F., Lionello, P., 2008. Climate change projections for the Mediterranean region. Glob. Planet. Chang. 63:90–104. https://doi.org/10.1016/j.gloplacha.2007.09.005.

Guo, J., 2002. Overflow risk analysis for stormwater quality control basins. J. Hydrol. Eng. 7 (6):428–434. https://doi.org/10.1061/(ASCE)1084-0699(2002)7:6(428).

Guzzetti, F., Cardinali, M., Reichenbach, P., 1996. The influence of structural setting and lithology on landslide type and pattern. Environmental and Engineering Geosciences, Vol. 2: 4, Winter 1996:pp. 531–555 https://doi.org/10.2113/gseegeosci.II.4.531.

Guzzetti, F., Malamud, B.D., Turcotte, D.L., Reichenbach, P., 2002. Power-law correlations of landslide areas in Central Italy. Earth Planet. Sci. Lett. 195:169–183. https://doi.org/10.1016/S0012-821X(01)00589-1.

Guzzetti, F., Reichenbach, P., Cardinali, M., Galli, M., Ardizzone, F., 2005. Probabilistic landslide hazard assessment at the basin scale. Geomorphology 72:272–299. https://doi.org/10.1016/j.geomorph.2005.06.002.

Guzzetti, F., Peruccacci, S., Rossi, M., Stark, C.P., 2007. Rainfall thresholds for the initiation of landslides in central and southern Europe. Meteorog. Atmos. Phys. 98:239–267. https://doi.org/10.1007/s00703-007-0262-7.

Guzzetti, F., Ardizzone, F., Cardinali, M., Galli, M., Reichenbach, P., Rossi, M., 2008a. Distribution of landslides in the Upper Tiber River basin, central Italy. Geomorphology 96: 105–122. https://doi.org/10.1016/j.geomorph.2007.07.015.

Guzzetti, F., Peruccacci, S., Rossi, M., Stark, C.P., 2008b. The rainfall intensity-duration control of shallow landslides and debris flows: an update. Landslides 5 (1):3–17. https://doi.org/10.1007/s10346-007-0112-1.

Hanson, R.T., Flint, L.E., Flint, A.L., Dettinger, M.D., Faunt, C.C., Cayan, D., Schmid, W., 2012. A method for physically based model analysis of conjunctive use in response to potential climate changes. Water Resour. Res. 48:W00L08. https://doi.org/10.1029/2011WR010774.

von Hardenberg, J., Ferraris, L., Rebora, N., Provenzale, A., 2007. Meteorological uncertainty and rainfall downscaling. Nonlinear Process. Geophys. 14:193–199. https://doi.org/10.5194/npg-14-193-2007.

von Hardenberg, J., Parodi, A., Pieri, A.B., Provenzale, A., 2015. Impact of microphysics and convective parameterizations on dynamical downscaling for the European domain. In: M. Lollino, G and Manconi, A and Clague, J and Shan, W and Chiarle M (Ed.), Engineering Geology for Society and Territory - Volume 1. Springer International Publishing:pp. 209–213 https://doi.org/10.1007/978-3-319-09300-0_40.

Harris, D., Menabde, M., Seed, A., Austin, G., 1996. Multifractal characterization of rain fields with a strong orographic influence. J. Geophys. Res. 101 (D21):26405–26414. https://doi.org/10.1029/96JD01656.

Hawkins, E., Sutton, R., 2009. The potential to narrow uncertainty in regional climate predictions. Bull. Am. Meteorol. Soc. 90 (8):1095–1107. https://doi.org/10.1175/2009BAMS2607.1.

Hergarten, S., 2012. Topography-based modeling of large rockfalls and application to hazard assessment. Geophys. Res. Lett. 39, L13402. https://doi.org/10.1029/2012GL052090.

Hong, S.-Y., Lim, J.-O.J., 2006. The WRF single-moment 6-class microphysics scheme (WSM6). J. Korean Meteor. Soc. 42 (2), 129–151.

Hovius, N., Stark, C.P., Allen, P.A., 1997. Sediment flux from a mountain belt derived by landslide mapping. Geology 25:231–234. https://doi.org/10.1130/0091-7613(1997)025<0231:SFFAMB>2.3.CO;2.

IPCC Intergovernmental Panel on Climate Change, 2014. Climate Change 2014: Synthesis Report. Contribution of Working Groups I, II and III to the Fifth Assessment Report of the Intergovernmental Panel on Climate Change, Geneva, Switzerland 151 pp. https://www.ipcc.ch/report/ar5/syr.

Kain, J.S., Fritsch, J.M., 1990. A one-dimensional entraining/detraining plume model and its application in convective parameterization. J. Atmos. Sci. 47 (23):2784–2802. https://doi.org/10.1175/1520-0469(1990)047%3C2784:AODEPM%3E2.0.CO;2.

Katz, O., Aharonov, E., 2006. Landslides in vibrating sand box: what controls types of slope failure and frequency magnitude relations? Earth Planet. Sci. Lett. 247:280–294. https://doi.org/10.1016/j.epsl.2006.05.009.

Klar, A., Aharonov, E., Kalderon-Asael, B., Katz, O., 2011. Analytical and observational relations between landslide volume and surface area. J. Geophys. Res. 116, F02001. https://doi.org/10.1029/2009JF001604.

Knutti, R., Furrer, R., Tebaldi, C., Cermak, J., Meehl, G.A., 2010. Challenges in combining projections from multiple climate models. J. Clim. 23:2739–2758. https://doi.org/10.1175/2009JCLI3361.1.

Kotlarski, S., et al., 2014. Regional climate modeling on European scales: a joint standard evaluation of the URO-CORDEX RCM ensemble. Geosci. Model Dev. 7 (4):1297–1333. https://doi.org/10.5194/gmd-7-1297-2014.

LoPresti, A., Charland, A., Woodard, D., Randerson, J., Diffenbaugh, N.S., Davis, S.J., 2015. Rate and velocity of climate change caused by cumulative carbon emissions. Environ. Res. Lett. 10, 095001. https://doi.org/10.1088/1748-9326/10/9/095001.

Malamud, B., Turcotte, D.L., Guzzetti, F., Reichenbach, P., 2004. Landslide inventories and their statistical properties. Earth Surf. Process. Landf. 29:687–711. https://doi.org/10.1002/esp.1064.

Malet, J.-P., Van Asch, T.W., Van Beek, R., Maquaire, O., 2005. Forecasting the behaviour of complex landslides with a spatially distributed hydrological model. Nat. Hazards Earth Syst. Sci. 5:71–85. https://doi.org/10.5194/nhess-5-71-2005.

Maraun, D., 2016. Curr. Clim. Change Rep. 2 (4):211–220. https://doi.org/10.1007/s40641-016-0050-x.

Melillo, M., Brunetti, M.T., Peruccacci, S., Gariano, S.L., Guzzetti, F., 2015. An algorithm for the objective reconstruction of rainfall events responsible for landslides. Landslides 12:311–320. https://doi.org/10.1007/s10346-014-0471-3.

Melillo, M., Brunetti, M.T., Peruccacci, S., Gariano, S.L., Guzzetti, F., 2016. Rainfall thresholds for the possible landslide occurrence in Sicily (southern Italy) based on the automatic reconstruction of rainfall events. Landslides 13:165–172. https://doi.org/10.1007/s10346-015-0630-1.

Mendlik, T., Gobiet, A., 2016. Selecting climate simulations for impact studies based on multivariate patterns of climate change. Clim. Chang. 135:381–393. https://doi.org/10.1007/s10584-015-1582-0.

Mergili, M., Marchesini, I., Alvioli, M., Metz, M., Schneider-Muntau, B., Rossi, M., Guzzetti, F., 2014. A strategy for GIS-based 3-D slope stability modelling over large areas. Geosci. Model Dev. 7:2969–2982. https://doi.org/10.5194/gmd-7-2969-2014.

Montgomery, D.R., Dietrich, W.E., 1994. A physically-based model for the topographic control on shallow landsliding. Water Resour. Res. 30:1153–1171. https://doi.org/10.1029/93WR02979.

Peruccacci, S., Brunetti, M.T., Luciani, S., Vennari, C., Guzzetti, F., 2012. Lithological and seasonal control on rainfall thresholds for the possible initiation of landslides in central Italy. Geomorphology 139-140:79–90. https://doi.org/10.1016/j.geomorph.2011.10.005.

Peruccacci, S., Brunetti, M.T., Gariano, S.L., Melillo, M., Rossi, M., Guzzetti, F., 2017. Rainfall thresholds for possible landslide occurrence in Italy. Geomorphology 290:39–57. https://doi.org/10.1016/j.geomorph.2017.03.031.

Pieri, A.B., von Hardenberg, J., Parodi, A., Provenzale, A., 2015. Sensitivity of precipitation statistics to resolution, microphysics, and convective parameterization: a case study with the high-resolution WRF climate model over Europe. J. Hydrometeorol. 16 (4):1857–1872. https://doi.org/10.1175/JHM-D-14-0221.1.

Raia, S., Alvioli, M., Rossi, M., Baum, R.L., Godt, J.W., Guzzetti, F., 2014. Improving predictive power of physically based rainfall-induced shallow landslide models: a probabilistic approach. Geosci. Model Dev. 7:495–514. https://doi.org/10.5194/gmd-7-495-2014.

Rebora, N., Ferraris, L., von Hardenberg, J., Provenzale, A., 2006a. Rainfall downscaling and flood forecasting: a case study in the Mediterranean area. Nat. Hazards Earth Syst. Sci. 6:611–619. https://doi.org/10.5194/nhess-6-611-2006.

Rebora, N., Ferraris, L., von Hardenberg, J., Provenzale, A., 2006b. RainFARM: rainfall downscaling by a filtered autoregressive model. J. Hydrometeorol. 7:724–738. https://doi.org/10.1175/JHM517.1.

Reid, M.E., Christian, S.B., Brien, D.L., Henderson, S.T., 2015. Scoops3D—software to analyze three-dimensional slope stability throughout a digital landscape. U.S. Geological Survey Techniques and Methods, Book 14 :p. 218 (Chap. A1). https://doi.org/10.3133/tm14A1.

Rianna, G., Zollo, A.L., Tommasi, P., Paciucci, M., Comegna, L., Mercogliano, P., 2014. Evaluation of the effects of climate changes on landslide activity of Orvieto clayey slope. Procedia Earth Plan. Sci. 9:54–63. https://doi.org/10.1016/j.proeps.2014.06.017.

Rianna, G., Reder, A., Mercogliano, P., Pagano, L., 2017. Evaluation of variations in frequency of landslide events affecting pyroclastic covers in Campania region under the effect of climate changes. Hydrology 2017 (4):34. https://doi.org/10.3390/hydrology4030034.

Rigon, R., Bertoldi, G., Over, T., 2006. GEOtop: a distributed hydrological model with coupled water and energy budgets. J. Hydrometeorol. 7:371–388. https://doi.org/10.1175/JHM497.1.

Roberds, W., 2005. Estimating temporal and spatial variability and vulner- ability. In: Hungr, O., Fell, R., Couture, R., Eberhardt, E. (Eds.), Landslide Risk Management. A.A. Balkema Publishers, Rotterdam, pp. 129–157.

Rossi, M., Witt, A., Guzzetti, F., Malamud, B.D., Peruccacci, S., 2010. Analysis of historical landslide time series in the Emilia-Romagna region, northern Italy. Earth Surf. Process. Landf. 35:1123–1137. https://doi.org/10.1002/esp.1858.

Saito, H., Nakayama, D., Matsuyama, H., 2010. Relationship between the initiation of a shallow landslide and rainfall intensity—Duration thresholds in Japan. Geomorphology 118:167–175. https://doi.org/10.1016/j.geomorph.2009.12.016.

Shamsudin, S., Dan'azumi, S., Aris, A., 2010. Effect of storm separation time on rainfall characteristics-a case study of Johor, Malaysia. Eur. J. Sci. Res. 45 (2), 162–167.

Simoni, S., Zanotti, F., Bertoldi, G., Rigon, R., 2008. Modelling the probability of occurrence of shallow landslides and channelized debris flows using GEOtop-FS. Hydrol. Process. 22:532–545. https://doi.org/10.1002/hyp.6886.

Simonovic, S.P., Schardong, A., Sandinik, D., Srivastav, R., 2016. A web-based tool for the development of intensity duration frequency curves under changing climate. Environ. Model. Softw. 81:136–153. https://doi.org/10.1016/j.envsoft.2016.03.016.

Stark, C.P., Guzzetti, F., 2009. Landslide rupture and the probability distribution of mobilized debris volumes. J. Geophys. Res. 114:F00A02. https://doi.org/10.1029/2008JF001008.

Tarquini, S., Vinci, S., Favalli, M., Doumaz, F., Fornaciai, A., Nannipieri, L., 2012. Release of a 10-m-resolution DEM for the Italian territory: Comparison with global-coverage DEMs and anaglyph-mode exploration via the web. Comput. Geosci. 38:168–170. https://doi.org/10.1016/j.cageo.2011.04.018.

Teutschbein, C., Seibert, J., 2012. Bias correction of regional climate model simulations for hydrological climate-change impact studies: review and evaluation of different methods. J. Hydrol. 456–457:12–29. https://doi.org/10.1016/j.jhydrol.2012.05.052.

Thomson, A.M., Calvin, K.V., Smith, S.J., Kyle, G.P., Volke, A., Patel, P., Delgado-Arias, S., Bond-Lamberty, B., Wise, M.A., Clarke, L.E., Edmonds, J.A., 2011. RCP4.5: a pathway for stabilization of radiative forcing by 2100. Clim. Chang. 109:77–94. https://doi.org/10.1007/s10584-011-0151-4.

Turco, M., Palazzi, E., von Hardenberg, J., Provenzale, A., 2015. Observed climate change hotspots. Geophys. Res. Lett. 42:3521–3528. https://doi.org/10.1002/2015GL063891.

Viet, T.T., Alvioli, M., Lee, G., Hyun Uk, A., 2018. Three-dimensional, time-dependent modeling of rainfall-induced landslides over a digital landscape: a case study. Landslides in press. https://doi.org/10.1007/s10346-017-0931-7.

Von Ruette, J., Lehmann, P., Or, D., 2013. Rainfall-triggered shallow landslides at catchment scale – threshold mechanics-based modeling for abruptness and localization. Water Resour. Res. 49:1–20. https://doi.org/10.1002/wrcr.20418.

Wilcke, R.A.I., Bärring, L., 2016. Selecting regional climate scenarios for impact modelling studies. Environ. Model. Softw. 78:191–201. https://doi.org/10.1016/j.envsoft.2016.01.002.

Witt, A., Malamud, B.D., Rossi, M., Guzzetti, F., Peruccacci, S., 2010. Temporal correlations and clustering of landslides. Earth Surf. Process. Landf. 35:1138–1156. https://doi.org/10.1002/esp.1998.